Curvature effects in the spectral dimension of spin foams

Alexander F. Jercher[1,3,4,*] Sebastian Steinhaus,[1,†] and Johannes Thürigen[2,‡]

[1]*Theoretisch-Physikalisches Institut, Friedrich-Schiller-Universität Jena*
Max-Wien-Platz 1, 07743 Jena, Germany, EU
[2]*Mathematisches Institut der Westfälischen Wilhelms-Universität Münster*
Einsteinstraße 62, 48149 Münster, Germany, EU
[3]*Arnold Sommerfeld Center for Theoretical Physics, Ludwig-Maximilians-Universität München*
Theresienstrasse 37, 80333 München, Germany, EU
[4]*Munich Center for Quantum Science and Technology (MCQST)*
Schellingstrasse 4, 80799 München, Germany, EU

It has been shown in [S. Steinhaus and J. Thürigen, Phys. Rev. D **98,** 026013 (2018)] that a class of restricted spin foam models can feature a reduced spectral dimension of space-time. However, it is still an open question how curvature affects the flow of the spectral dimension. To answer this question, we consider another class of restricted spin foam models, so-called spin foam frusta, which naturally exhibit oscillating amplitudes induced by curvature, as well as an extension of the parameter space by a cosmological constant. Numerically computing the spectral dimension of one-periodic frusta geometries using extrapolated quantum amplitudes, we find that quantum effects lead to a small change of spectral dimension at small scales and an agreement to semiclassical results at larger scales. Adding a cosmological constant Λ, we find additive corrections to the nonoscillating result at the diffusion scale $\tau \sim 1/\sqrt{\Lambda}$. Extending to two-periodic configurations, we observe a reduced effective dimension, the form of which sensitively depends on the values of the gravitational constant G and the cosmological constant Λ. We provide an intuition for our results based on an analytical estimate of the spectral dimension. Furthermore, we present a simplified integrable model with oscillating measure that qualitatively explains the features found numerically. We argue that there exists a phase transition in the thermodynamic limit which crucially depends on the parameters G and Λ. In principle, the dependence on G and Λ presents an exciting opportunity to infer phenomenological insights about quantum geometry from measurement of the spectral dimension.

I. INTRODUCTION

Deriving observable consequences is crucial for understanding the structure of any quantum theory of gravity and of quantum space-time itself, especially when formulated using discrete structures, such as in the approaches of loop quantum gravity [1,2], spin foams [3], tensorial group field theories [4–6], causal dynamical triangulations [7,8], and causal set theory [9,10]. The spectral dimension, derived from the spectrum of the Laplacian on quantum space-time, has proven to be an informative phenomenological quantity.

This observable provides a notion of an effective dimension of emergent space-time on different scales. On the one hand, it allows for a consistency check that the space-times obtained from quantum gravity exhibit the observed dimension of $D = 4$ at large length scales. This is

already highly nontrivial as various approaches only yield fractal or two-dimensional geometries [11,12]. On the other hand, new small-scale effects beyond classical continuum gravity, sourced by the quantum nature of space-time, can be examined. Most prominently, a dimensional flow to values $0 < D < 4$ at small scales is an effect present in many quantum gravity approaches [13–28], possibly leaving observable traces in gravitational wave astronomy [29]. In any case, this phenomenon is interesting as it allows us to compare conceptually different approaches at small scales. Investigating the existence and structure of such a dimensional flow in spin foam quantum gravity [3], specifically using the restricted setting of spin foam frusta models [30,31], is the main objective of this article.

Spin foam models provide a path integral quantization of discretized geometries where the microscopic gravitational degrees of freedom are encoded in group representation labels and intertwiners. Although model defining amplitudes are defined rigorously and consistently on the

*[*]alexander.jercher@uni-jena.de
[†]sebastian.steinhaus@uni-jena.de
[‡]johannes.thuerigen@uni-muenster.de

quantum level, challenges remain to turn spin foam quantum gravity into a consistent computational formalism. While there is a clear relation to semiclassical discrete gravity on a local level [32–35], exploring the semiclassical regime of extended discrete structures is a subject of active research [36–42]. Moreover, a consistent quantum theory of gravity needs to be independent of any discretization chosen in the quantization procedure. Discretization independence of spin foams can be attained either in the group field theory formalism [4–6] or via a spin foam renormalization procedure [43–45]. Furthermore, in recent years, there has been promising progress in numerical methods [46] that tackle the challenge of performing calculations in spin foams from different angles [35–39,41,42,47–51]. Defining and explicitly computing the spectral dimension in spin foam models makes contact with these open questions and serves as a coarse characterization of the quantum space-times obtained therein.

A first attempt to determine the spectral dimension D_s of spin foams in [13] has been in the setting of spin foam cuboids [51–54], a restricted subclass of the Euclidean Engle-Pereira-Rovelli-Livine/Freidel-Krasnov (EPRL-FK) model [55,56] defined within the Kaminski-Kisielowski-Lewandowski extension to general two-complexes [57]. Therein, a restriction to $\mathcal{N}$-periodic geometric configurations proved crucial for numerically feasible calculations. At finite $\mathcal{N}$, the spectral dimension shows an intermediate value which depends on the choice of a face amplitude parameter α. In the limit $\mathcal{N} \to \infty$, the analytical results of [13] suggest that there is a phase transition from $D_s = 0$ to $D_s = 4$ at the point α_* where the amplitudes become scale invariant.

Although an important step towards control of the spectral dimension of spin foam quantum gravity, the results on spin foam cuboids [13] come with two major limitations. First, the spectral dimension is computed utilizing semiclassical amplitudes which capture only the large scale behavior correctly. Second, and most importantly, spin foam cuboids are inherently flat, reflected in the fact that the semiclassical action vanishes on critical points. As a consequence, cuboid amplitudes exhibit a simple semiclassical scaling behavior without curvature-induced oscillations. Overcoming these limitations is the main purpose of the present work.

Since the spectral dimension for the full EPRL-FK model currently exceeds computational capacities, we choose the so-called spin foam frusta model, introduced in [30] and further examined in [31,51,58], to include curvature effects and a nonvanishing cosmological constant. Though the underlying combinatorial structure is a hypercubic lattice, the intertwiners of the theory are restricted in such a way that the four-dimensional building blocks semiclassically describe four-frusta. These building blocks can be understood as a four-dimensional generalization of regular trapezoids, with three-cubes as base and top connected

by six boundary three-frusta. It has been shown in [30] that semiclassical spin foam frusta exhibit curvature if the three-cubes are of different size. Because of their strongly restricted geometry, frusta exhibit a discrete analogue of spatial homogeneity. Thus, frusta are promising candidates for a cosmological subsector of spin foam models [30]. At the same time, this homogeneity leads to simplifications of the Laplace operator, providing a feasible setting for numerical computations of the spectral dimension.

Extrapolating one-periodic frusta quantum amplitudes and computing the spectral dimension therewith, we discover a nontrivial flow of the spectral dimension, exhibiting an intermediate value which is controlled by the face amplitude parameter α. Compared to a semiclassical analysis, the quantum amplitudes lead to an additive correction to the spectral dimension at small scales. Adding a cosmological constant Λ and thus introducing oscillations to the amplitudes, we find additive corrections to the spectral dimension at diffusion scales $\tau \sim 1/\sqrt{\Lambda}$. Supported by analytical calculations, we can explain these effects from quantum amplitudes and Λ-oscillations in terms of an effective scaling behavior of the amplitudes. For two-periodic frusta amplitudes we observe an intricate dependence of the dimensional flow on Newton's constant G and Λ, showing the significant role of curvature. On these grounds, we argue for a phase transition in the large-$\mathcal{N}$ limit that crucially depends on the parameter values of α, G, and Λ.

We begin this article by setting up the spin foam frusta model, its semiclassical limit, and by defining the Laplace operator on frusta geometries. Thereafter, we present the concept of $\mathcal{N}$ periodicity, which has been introduced already in [13] and provide the formulas for computing the quantum spectral dimension. In Sec. III, we provide a method to extrapolate one-periodic quantum amplitudes. Using the resulting extrapolated amplitudes, we compute the one-periodic spectral dimension in Sec. IV A. Proceeding with semiclassical amplitudes, we extend the analysis of the spectral dimension to include a cosmological constant in Sec. IV B and finally to two-periodic configurations in Sec. IV C. Based on the analytical estimate of the spectral dimension presented in Sec. IV D, we provide a broader discussion of our results in Sec. V and give and conclude our work in Sec. VI with an outlook on possible future studies.

II. SPIN FOAM HYPERFRUSTA AND THE SPECTRAL DIMENSION

In this section we provide a brief introduction to the setting of the present work and, in particular, define the spectral dimension as a spin foam observable. Giving first the relevant formulas for classical hyperfrusta, we introduce spin foam frusta as restrictions of the Euclidean EPRL-FK model. Thereafter, we set up the classical spectral dimension in a discrete setting and translate these ideas to spin foam hyperfrusta.

A. Spin foam frusta

In the present work, we employ the Euclidean EPRL-FK model [55,56] with a Barbero-Immirzi parameter $\gamma_{BI} < 1$. Originally defined on a two-complex Γ dual to a triangulation, this model was later generalized to arbitrary two-complexes [57,59], which includes, in particular, the hypercuboidal structure we intend to work with. In the following, we introduce all the defining ingredients of the EPRL-FK model.

1. Definition of spin foam frusta

Given a two-complex Γ with vertices v, edges e, and faces f, we associate to it the following partition function:

$$Z = \sum_{j_f, \iota_e} \prod_f \mathcal{A}_f \prod_e \mathcal{A}_e \prod_v \mathcal{A}_v. \qquad (2.1)$$

The variables j_f denote irreducible SU(2) representations, frequently referred to as spins, and are assigned to the faces f of Γ. The ι_e are SU(2) intertwiners, i.e., elements in the invariant subspace of the tensor product of representations meeting at the edge e. $\mathcal{A}_f$, $\mathcal{A}_e$, and $\mathcal{A}_v$ are the face, edge, and vertex amplitudes, respectively, and we define them in the following.

Characteristic for Euclidean gravity, the local gauge group is SO(4), or its double cover Spin(4) $\cong$ SU(2) × SU(2), with SU(2) being a subgroup. A distinctive property of the Euclidean EPRL-FK model is the simplicity constraint which provides an embedding $Y_{\gamma_{BI}}$ of SU(2) into Spin(4) representations [55]. For $\gamma_{BI} < 1$, the explicit relation between SU(2) spins j and Spin(4) labels (j^+, j^-) is given by

$$j^{\pm} = \frac{|1 \pm \gamma_{BI}|}{2} j \in \frac{\mathbb{N}}{2}, \qquad (2.2)$$

with the condition that the $j^{\pm}$ are half-integers. For this map to be nonempty, γ_{BI} is required to be rational. Given a certain range of spins with N_{spin} configurations in total, only a certain number $N(\gamma_{BI})$ is allowed.[1] A plot for the ratio of $N(\gamma_{BI})$ and N_{spin} is given in Fig. 1.

Different face amplitudes are proposed in the literature,[2] the choice of which has direct consequences for the critical behavior of the partition function [61], as well as the spectral dimension [13]. We parametrize this ambiguity by $\alpha \in \mathbb{R}$ as

$$\mathcal{A}_f^{(\alpha)} = ((2j_f^+ + 1)(2j_f^- + 1))^{\alpha}. \qquad (2.3)$$

The edge amplitude of the model is introduced as a normalization factor

$$\mathcal{A}_e = \frac{1}{\|Y_{\gamma_{BI}}\iota_e\|^2} \qquad (2.4)$$

and the vertex amplitude is defined as

$$\mathcal{A}_v = \mathrm{Tr}\left(\bigotimes_{e \subset v} Y_{\gamma_{BI}}\iota_e\right), \qquad (2.5)$$

where the trace is understood so that either $(Y_{\gamma_{BI}}\iota_e)$ or $(Y_{\gamma_{BI}}\iota_e)^{\dagger}$ is contracted, depending on the edge e being ingoing or outgoing from the vertex v, respectively.

With the general definition of the model being set up, we now introduce two restrictions on the partition function, being of combinatorial and geometrical kinds. First, we assume that the two-complex Γ and thus also the

FIG. 1. Ratio of the number N of allowed configurations and the total number of spins N_{spins} for rational Barbero-Immirzi parameters $\gamma_{BI} = \frac{p}{q}$ with $q \in \{1, 2, ..., 50\}$ and $p \in \{1, 2, ..., q-1\}$.

---

[1]The ratio $N(\gamma_{BI})/N_{spin}$ for $\gamma_{BI} = \frac{p}{q} \in \mathbb{Q}$ is either $1/q$ or $1/2q$ depending on whether $q \pm p$ is even or odd which explains the asymmetry in Fig. 1 (e.g., for $q = 5$ we have ratio $1/5$ for $p = 1, 3$ while $1/10$ for $p = 2, 4$). More precisely, let $q \in \mathbb{N}$ and $p \in \{1, 2, ..., q-1\}$ but $p \perp q$ (coprime, otherwise there are smaller p', q' with $\gamma_{BI} = \frac{p}{q} = \frac{p'}{q'}$ to be considered). Then the EPRL condition equation (2.2) yields $\frac{q \pm p}{2q} n \in \mathbb{N}$. Write $\frac{q \pm p}{2q} = \frac{r}{s}$ with $r \perp s$. Then the condition is fulfilled if $\frac{n}{s} \in \mathbb{N}$, that is, for every s's spin. Thus, the ratio is $N/N_{spins} = s$ and there are two cases for given q, either $s = q$ or $s = 2q$. To see this, note first that $q + p \perp 2q$ iff $2q - (q+p) = q - p \perp 2q$, thus the two cases $\pm \gamma_{BI}$ give the same s. Then, $q + p$ and $2q$ have a common divisor iff $q + p$ is even in which case $s = q$ and this happens for every second p for a given q.

[2]Following [60], the two most common choices for the face amplitude in the Riemannian setting are either the dimension of the Spin(4) representation or the dimension of the SU(2) representation. Viewing the Euclidean EPRL-model as a constrained Spin(4)-BF theory, the dimension factor is a result of expanding δ distributions on Spin(4) in terms of representations. Choosing the SU(2) dimension instead can be motivated physically, as argued in [60]. The two choices correspond to $\alpha = 1$ and $\alpha = \frac{1}{2}$, respectively. Clearly, the parametrization of Eq. (2.3) constitutes a continuous interpolation between these two choices.
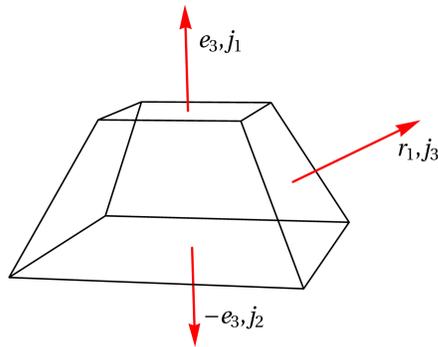
FIG. 2. A regular three-frustum with squares in the e_3 plane. The slope angle ϕ is defined between e_3 and the r_l.

FIG. 3. Boundary of a four-frustum given by two three-cubes of, generically, different size and six equal three-frusta.

discretization is hypercubic. As we will see later in Sec. II B 1 and Sec. II B 2, respectively, the choice of a hypercubic lattice is convenient for defining a discrete Laplace operator as well as for considering periodic configurations. Notice, that this choice of combinatorics does not imply a reduction to hypercubic geometries.

On the geometrical side, we introduce the restriction to regular four-frustum geometries [30]. The boundary of such configurations consists of two cubes of *a priori* different size and six equal three-frusta. It is therefore reasonable to impose a three-frustum shape on the Livine-Speziale coherent intertwiners [62], since these objects are naturally peaked on the geometry of three-dimensional polyhedra.[3] An explicit expression for three-frustum intertwiners is given by

$$
\iota_{j_1 j_2 j_3} = \int_{\mathrm{SU}(2)} \mathrm{d}g\, g \triangleright \left(|j_1, \hat{e}_3\rangle \otimes |j_2 - \hat{e}_3\rangle \overset{3}{\underset{l=0}{\bigotimes}} |j_3, \hat{r}_l\rangle \right), \quad (2.6)
$$

where the case $j_1 = j_2 = j_3$ reduces $\iota_{j_1 j_2 j_3}$ to a cubical intertwiner [63]. In Eq. (2.6), "$\triangleright$" denotes the action of an SU(2)-group element on coherent states in representation space, $\hat{e}_3$ is the unit vector in $\mathbb{R}^3$ along the axis e_3 and $\hat{r}_l = \mathrm{e}^{-i\frac{\pi}{4}l\sigma_3}\mathrm{e}^{-i\frac{\phi}{2}\sigma_2} \triangleright \hat{e}_3$ for $l \in \{0, 1, 2, 3\}$. A depiction of a regular three-frustum is given in Fig. 2.

A semiclassical three-frustum can be understood as the generalization of a regular trapezoid to three dimensions, characterized by three areas j_1, j_2, and j_3 of the base and top square and of the bounding trapezoids, respectively. Another convenient parametrization is given by j_1, j_2 and the slope angle ϕ. The relation between the spins and ϕ is given by

$$
\cos(\phi) = \frac{j_1 - j_2}{4j_3}, \quad (2.7)
$$

which follows from the closure condition. Clearly, for the slope angle to be well defined, the condition $-1 \leq \frac{j_1 - j_2}{4j_3} \leq 1$ is required to hold.

Gluing two cubes and six three-frusta as indicated above, one obtains a four-dimensional hyperfrustum. The two three-cubes lie in separated spatial hypersurfaces at the base and top, connected by the six three-frusta. A visualization of the unwrapped boundary of a single four-frustum is given in Fig. 3.

As a whole complex, the discretization can be understood as a slicing, where the nth thick slice is bounded by two spatial hypersurfaces cubulated by three-cubes with area j_n and j_{n+1}, respectively, and connected by three-frusta with spatio-"temporal" areas given by k_n. Because of the gluing conditions, the spins j_n, j_{n+1} and k_n are constant throughout a whole slice. Therefore, spin foam configurations of hyperfrusta are translation invariant in spatial directions. This implies that the volume of cubes changes only between different spatial hypersurfaces, i.e., in temporal direction. This makes hyperfrustum spin foams well suited for the description of discrete classical cosmology, where we refer to [30] for further details.

2. Asymptotics of spin foam frusta

In general, the quantum amplitudes defined by Eqs. (2.5) and (2.4) are highly involved functions of the representation labels. To find a suitable approximation and to obtain an analytical expression for later purposes, we present in the following the results of an asymptotic analysis [32,33] of the frustum quantum amplitudes [30]. The regime of large representation labels is interpreted as the semiclassical sector of the theory, thereby connecting it to classical discrete gravity [64].

---

[3]Notice that the frustum symmetry reduction is a restriction on the quantum level, as it is imposed on the coherent intertwiners. Such a procedure is distinct from a classical symmetry reduction followed by quantization. We remark further, that lifting this restriction is unfortunately not straightforward. As elaborated in Sec. VI, a triangulation offers a more manageable setting to study models with less symmetries.

Introducing a uniform rescaling of spins, $j_i \to \lambda j_i$, and sending $\lambda \to \infty$, the quantum face amplitude in Eq. (2.3) is approximated by

$$\mathcal{A}_f = [(1 - \gamma_{\mathrm{BI}}{}^2)j_n^2]^\alpha. \qquad (2.8)$$

To find the asymptotics of the vertex and the edge amplitude $\mathcal{A}_i$, we notice the factorization property $\mathcal{A}_i = \mathcal{A}_i^+ \mathcal{A}_i^-$ with $\mathcal{A}_i^\pm$ being the SU(2) amplitudes evaluated on the spins $j^\pm$. This is a result of the $Y_{\gamma_{\mathrm{BI}}}$ map entering Eqs. (2.4) and (2.5) which holds for $\gamma_{\mathrm{BI}} < 1$. We rewrite an amplitude $\mathcal{A}_i^\pm$ as an integral of a complex exponential of an action which scales linearly in λ. Then one can apply an extended stationary phase approximation [32] in the limit $\lambda \to \infty$ which consists of evaluating the integrand on the critical points of the action, multiplied by the inverse square root of the Hessian and some factors of π. Following this procedure for the SU(2)-vertex amplitude, one finds [30]

$$\mathcal{A}_v^{\mathrm{SU}(2)}(j_n, j_{n+1}, k_n) = \frac{1}{2^{21/2}\pi^{7/2}}\left(\frac{e^{\frac{i}{G}S_R}}{\sqrt{-D}} + \frac{e^{-\frac{i}{G}S_R}}{\sqrt{-D^*}}\right), \qquad (2.9)$$

where D is the determinant of the Hessian, defined as

$$\begin{aligned} D := {} & 16j_n^3 j_{n+1}^3 k_n^{15} K(K - iK^2 + iQ)^3 \\ & \times (1 + K^2 - 2Q)^3 (K + i)^6 (K - 3i)^2 \\ & \times (1 + 3K^2 - 2Q - 2iK(Q - 1))^3, \qquad (2.10) \end{aligned}$$

with

$$Q := 2 + \frac{j_n + j_{n+1}}{2k_n}, \qquad \theta := \arccos\frac{1}{\tan\phi},$$

$$K := \sqrt{-\cos 2\phi}. \qquad (2.11)$$

Furthermore, S_R is the Regge action [65] of a single hyperfrustum and given by

$$S_R = 6(j_n - j_{n+1})\left(\frac{\pi}{2} - \theta\right) + 12k_n\left(\frac{\pi}{2} - \arccos(\cos^2(\theta))\right) \qquad (2.12)$$

and G is the gravitational constant, which has been added by hand as in [31].[4] Given Eq. (2.9), the semiclassical Spin(4)-vertex amplitude is

$$\mathcal{A}_v = \frac{1}{\pi^7(1 - \gamma_{\mathrm{BI}}{}^2)^{21/2}}\left(\frac{e^{\frac{i}{G}S_R}}{-D} + \frac{e^{-\frac{i}{G}S_R}}{-D^*} + 2\frac{\cos(\frac{\gamma_{\mathrm{BI}}}{G}S_R - \frac{\Lambda}{G}V^{(4)})}{\sqrt{DD^*}}\right), \qquad (2.13)$$

where we have introduced a cosmological constant Λ, following the work of [66,67]. Therein, the quantum amplitudes are deformed in a heuristic fashion by a real parameter which, in a semiclassical limit, can be related to a cosmological constant of either sign. It enters with the four-volume $V^{(4)}$ of a hyperfrustum, defined in Eq. (2.28) below, which is strictly positive and thus does not correspond to a signed volume.[5]

Repeating the analysis, the semiclassical SU(2)-edge amplitude is given by

$$\begin{aligned} & \mathcal{A}_e^{\mathrm{SU}(2)}(j_n, j_{n+1}, k_n) \\ & = 2\sqrt{2\pi}\sqrt{\frac{k_n \sin^2(\phi)}{2}}(j_n + j_{n+1} + 2k_n(1 - \cos^2(\phi)))^2. \end{aligned} \qquad (2.14)$$

Consequently, the semiclassical approximation to the Spin(4)-edge amplitude, Eq. (2.4), is

$$\begin{aligned} \mathcal{A}_e = {} & \pi(1 - \gamma_{\mathrm{BI}}{}^2)^{3/2}\frac{k_n \sin^2(\phi)}{2}(j_n + j_{n+1} \\ & + 2k_n(1 - \cos^2(\phi)))^2. \qquad (2.15) \end{aligned}$$

For general discretizations an edge is shared by two vertices. Special to a hypercubic lattice, every face is shared by four vertices. These two facts allow us to define a dressed vertex amplitude

$$\hat{\mathcal{A}}_v = \prod_{f \supset v}\mathcal{A}_f^{1/4}\prod_{e \supset v}\mathcal{A}_e^{1/2}\mathcal{A}_v, \qquad (2.16)$$

such that the amplitude of the whole complex can be written as the product of dressed vertex amplitudes.

Even in the presence of oscillations, originating from a nonvanishing cosmological constant or a nonvanishing Regge curvature, the dressed vertex amplitudes behave under uniform rescaling as

$$\hat{\mathcal{A}}_v(\lambda j_n, \lambda j_{n+1}, \lambda k_n) \sim \lambda^{12\alpha - 9}. \qquad (2.17)$$

Comparing $\hat{\mathcal{A}}_v$ to the dressed vertex amplitude of spin foam cuboids [63], we see that the this scaling is the same. However, $\hat{\mathcal{A}}_v$ is *not* a homogeneous function in the spins,

---

[4]In units where $\hbar = c = 1$, the gravitational constant has the dimension of area. Considering the j_n as mere representation labels, only Gj_n has the interpretation of an area. For the majority of the spin foam literature, the spins are implicitly understood to have the dimension of area and therefore implicitly depend on G [31].

[5]Notice, that this positive quantity is the same quantity that enters the definition of the Laplace operator in Eq. (2.26). The cosmological constant term enters with a cosine in the quantum amplitudes since the critical points correspond to the two orientations.

due to the two types of oscillations in Eq. (2.16), which are not present in the case of cuboids. As a consequence, we cannot deduce that $\alpha = \frac{3}{4}$ is a point of scale invariance of the frusta model.

B. Spectral dimension of spin foam frusta

In this section, we introduce the notion of spectral dimension, first classically on semiclassical frusta geometries. After restricting to so-called $\mathcal{N}$-periodic configurations, we set up the spectral dimension of spin foam frusta as a quantum expectation value.

1. Spectral dimension and semiclassical geometry of hyperfrusta

The spectral dimension serves as an effective measure of the dimension of a space. In the continuum, consider a Riemannian manifold $(\mathcal{M}, g)$ together with the heat kernel $K(x, x_0; \tau)$ which is a solution of the heat equation [14]

$$\partial_\tau K(x, x_0; \tau) = \Delta K(x, x_0; \tau). \qquad (2.18)$$

Here, $x, x_0 \in \mathcal{M}$, and τ provides a measure of the size of the probed region, often referred to as diffusion time. The classical spectral dimension $D_s^{cl}(\tau)$ is then extracted from the scaling of the return probability

$$P(\tau) := \int_{\mathcal{M}} dx \sqrt{g} K(x, x; \tau), \qquad (2.19)$$

by the relation

$$D_s^{cl}(\tau) := -2 \frac{d \log P(\tau)}{d \log \tau}. \qquad (2.20)$$

Clearly, the return probability implicitly depends on the metric g and therefore is a functional of the geometry. Thus, in a quantum gravity path integral picture with partition function

$$Z = \int dg e^{iS_{EH}[g]}, \qquad (2.21)$$

where $S_{EH}[g]$ is the Einstein-Hilbert action, the expectation value of the return probability is

$$\langle P(\tau) \rangle = \frac{1}{Z} \int dg P(\tau) e^{iS_{EH}[g]}. \qquad (2.22)$$

Consequently, one defines the spectral dimension as

$$D_s(\tau) := -2 \frac{d \log \langle P(\tau) \rangle}{d \log \tau}. \qquad (2.23)$$

Notice, that we do not compute $\langle D_s^{cl}(\tau) \rangle$ but define the quantum spectral dimension as the scaling of $\langle P(\tau) \rangle$.

To translate these continuum notions to the context of spin foams, we introduce now a discrete formulation of the Laplace operator, the return probability, and ultimately the spectral dimension. Assuming that the space $\mathcal{M}$ is discretized on a hypercubic lattice, we denote vertices in the dual graph Γ by $\vec{n} \in \mathbb{Z}^4$. Interpreting the return probability in Eq. (2.19) as the trace over the heat kernel, the discrete return probability is simply given by [68,69]

$$P(\tau) = \sum_{\vec{n} \in \Gamma} K(\vec{n}, \vec{n}, \tau). \qquad (2.24)$$

Then, one can rewrite the return probability as [69]

$$P(\tau) = \sum_{\lambda \in spec(\Delta)} e^{-\tau\lambda}, \qquad (2.25)$$

where $spec(\Delta)$ is the spectrum of the discrete Laplacian. Consequently, to obtain the spectral dimension, knowledge of the full spectrum on the whole lattice is required.

Following [68], the notion of an exterior derivative and a Laplace operator can be defined on general cellular complexes, using methods of discrete exterior calculus [70]. To that end, one introduces a scalar test field[6] discretized on the complex, which can be placed either on the vertices of the discretization or on its dual vertices. The strategy we follow here is to consider the scalar field $\phi_{\vec{n}}$ on dual[7] vertices of the complex Γ. From the continuum perspective, this case can be obtained by integrating a smooth scalar field over the region of a four-cell. Finally the discrete Laplacian is defined by its action on the scalar test field $\phi_{\vec{n}}$ [69]

$$-(\Delta\phi)_{\vec{n}} = -\sum_{\vec{m}\sim\vec{n}} \Delta_{\vec{n}\,\vec{m}}(\phi_{\vec{n}} - \phi_{\vec{m}})$$

$$= \frac{1}{V_{\vec{n}}^{(4)}} \sum_{\vec{m}\sim\vec{n}} \frac{V_{\vec{n}\,\vec{m}}^{(3)}}{l_{\vec{n}\,\vec{m}}^*} (\phi_{\vec{n}} - \phi_{\vec{m}}), \qquad (2.26)$$

where the sum runs over all adjacent vertices $\vec{m}$, indicated by "$\sim$". $\Delta_{\vec{n}\,\vec{m}}$ are the coefficients of the discrete Laplacian, which can be split into a diagonal part and a part which is proportional to the adjacency matrix of the complex Γ. $V_{\vec{n}\,\vec{m}}^{(3)}$ and $l_{\vec{n}\,\vec{m}}^*$ indicate the three-volume and the dual edge length, of $(\vec{n}\,\vec{m})$, respectively. The positive four-volume of the frustum dual to $\vec{n} \in \Gamma$ is denoted by $V_{\vec{n}}^{(4)}$ and is the same

---

[6]Importantly, test fields should not be confused with physical fields, minimally coupled to spin foams [54]. In particular, a test field does not have to satisfy spatial homogeneity even if the spin foam is fixed to spatially homogeneous configurations. Also, $\mathcal{N}$ periodicity, which we are going to introduce down below, does not need to be fulfilled by $\phi_{\vec{n}}$.

[7]Other choices work equally well. For example, in [54], a scalar field is placed on the vertices of the discretization. Beyond scalar fields, other tensor or p-form fields might yield different results for "generalized" spectral dimensions, though [25].

four-volume that accompanies the cosmological constant in the vertex amplitude of Eq. (2.13). Going beyond the scope of this work, we do not consider the possibility of working with oriented spin foam amplitudes and with signed four-volumes in the Laplace operator.

As discussed in detail in [69], the definition of volume and dual edge length and thus that of a discrete Laplacian is not unique in general. For constructing the dual two-complex, we pursue the following strategy. In four-dimensional Euclidean space, we orient a four-frustum along the t axis such that the two cubes lie in a constant-t hypersurface. Vertices of the dual lattice are then obtained by forming the average of the corner points of the four-frustum. Consequently, these points lie on the t axis on half of the four-frustum height. Dual edges, "spacelike" and "timelike," are chosen to be orthogonal on the faces of the four-frustum such that their lengths are minimal.[8] Notice that these definitions do not correspond to a barycentric construction. The distance between barycentric vertices would yield the dual edge lengths we obtain below, rescaled by a constant factor. For the return probability, such a constant prefactor can be absorbed into the scale τ and thus has no physical effect.

In the following, we define the geometric quantities that enter Eq. (2.26), based on the construction of the dual lattice discussed above. Thereby, we adopt the notation for which, in the nth "slice," the spins j_n, j_{n+1} refer to the area of the lower and upper cube, respectively, and where k_n labels the spatiotemporal area of boundary three-frusta.

First, we notice that the four-dimensional dihedral angles imply the following restriction on the possible spin values for each slice [51]:

$$-\frac{1}{\sqrt{2}} \le \frac{j_n - j_{n+1}}{4k_n} \le \frac{1}{\sqrt{2}}, \qquad (2.27)$$

posing a stronger condition than closure in Eq. (2.7). Volume and height of a four-frustum in the nth slice are, respectively, given by

$$V_n^{(4)} = \frac{1}{2} k_n (j_n + j_{n+1}) \sqrt{1 - \frac{(j_n - j_{n+1})^2}{8k_n^2}}, \qquad (2.28)$$

and

$$H_n = \frac{2k_n}{\sqrt{j_n} + \sqrt{j_{n+1}}} \sqrt{1 - \frac{(j_n - j_{n+1})^2}{8k_n^2}}. \qquad (2.29)$$

FIG. 4. Three-dimensional representation of a timelike dual edge, drawn in red, connecting the midpoints of two timelike separated frusta. From this representation, the duality of timelike edges and cubes (here squares) is immediate.

Since the boundary of a four-frustum consists of two types of building blocks, cubes, and three-frusta, we make a distinction in the following. This can be interpreted as separating the cases where $\vec{n}$ and $\vec{m}$ having spacelike or timelike separation.[9]

Timelike dual edges.—Three-dimensional volumes between the vertices $\vec{m}$ and $\vec{n}$, which connect the $(n-1)$th and nth slice, are simply given by the volume of cubes with area j_n

$$V_{\vec{m}\vec{n}}^{(3)} = j_n^{\frac{3}{2}}. \qquad (2.30)$$

Following the construction of a dual lattice outlined above, the length of dual edges is given as the half of the sum of heights of "past" and "future" hyperfrusta

$$
\begin{aligned}
l_\star^{\vec{m}\vec{n}} &= \frac{1}{2}(H^{n-1} + H^n) \\
&= \frac{k_{n-1}}{\sqrt{j_{n-1}} + \sqrt{j_n}} \sqrt{1 - \frac{(j_{n-1} - j_n)^2}{8k_{n-1}^2}} \\
&\quad + \frac{k_n}{\sqrt{j_n} + \sqrt{j_{n+1}}} \sqrt{1 - \frac{(j_n - j_{n+1})^2}{8k_n^2}}. \quad (2.31)
\end{aligned}
$$

A visualization of the dual edge and its length in a three-dimensional analog is given in Fig. 4.

This defines all the ingredients of the Laplace operator $\Delta_{\vec{m}\vec{n}}$ for neighboring vertices $\vec{m}, \vec{n}$ which have a timelike separation, and we use the notation Δ_{n-1n} in the following.

Spacelike dual edges.—In spacelike direction, so within a given slice n, four-frusta are connected with each other via boundary three-frusta. The corresponding three-volumes are given by

---

[8]Defining the dual edges in this way is convenient because of spatial homogeneity. In a more general setting, defining half dual edges by connecting midpoints of the four-frusta with midpoints of boundary hexahedra appears more natural.

[9]This designation needs to be used cautiously, since we work in a Riemannian context where there are no notions of causality.
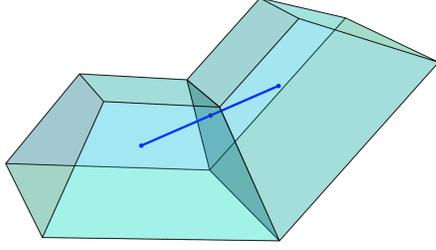
FIG. 5. Three-dimensional representation of a spacelike dual edge, drawn in blue, connecting the midpoints of two spacelike separated frusta. From this representation, the duality of spacelike edges and three-frusta (here trapezoids) is immediate.

$$V_{\vec{m}\,\vec{n}}^{(3)} = \frac{2k_n(j_n + \sqrt{j_n j_{n+1}} + j_{n+1})}{3(\sqrt{j_{n+1}} + \sqrt{j_n})}\sqrt{1 - \frac{(j_{n+1} - j_n)^2}{16k_n^2}}.$$

(2.32)

To obtain the length of spacelike dual edges, for which a visualization is given in Fig. 5, it suffices to project the geometry onto the plane spanned by the t axis and the dual edge. In this picture, the dual edge connects two glued trapezoids and is orthogonal with respect to the connecting face. For Θ the dihedral angle between the $(n + 1)$ cube and the boundary three-frustum, defined as [30]

$$\Theta_n = \arccos\left(\frac{1}{\tan(\phi_n)}\right),$$

(2.33)

the dual edge length is then given by

$$l_\star^{\vec{m}\,\vec{n}} = \frac{1}{2}(\sqrt{j_n} + \sqrt{j_{n+1}})\cos\left(\frac{\pi}{2} - \Theta_n\right).$$

(2.34)

We denote the components of the Laplacian $\Delta_{\vec{n}\,\vec{m}}$ with vertices $\vec{n}$ and $\vec{m}$ having a spacelike separation by Δ_{nn}.

Note that the definition of the discrete Laplacian requires a semiclassical interpretation of the geometry, as interpreting the spins j_n, k_n as areas is only valid in a semiclassical regime. However, in the computation of the spectral dimension, we assume that the definition $\Delta(j_n, k_n)$ holds for arbitrarily small spins, which can be seen as a continuation of the semiclassical Laplacian and provides *one* possible definition of Δ in the quantum regime. While there may be many valid definitions of microscopic Laplacians, they must converge to the semiclassical definition provided above.

2. $\mathcal{N}$ periodicity

Following the discussion in [13], evaluating the spectral dimension even in the setting of restricted spin foams is challenging because of two main reasons. First, the computation of the Laplacian's spectrum for many classical configurations is very costly. Second, evaluating the spin foam partition function scales exponentially with

the number of lattice sites. We elaborate on these numerical challenges in the following.

Let us consider the spectrum of the Laplacian for a given spin configuration first. As Eq. (2.25) shows, the return probability, and therefore the spectral dimension, requires full knowledge of the spectrum of the discrete Laplacian.[10] Given that the lattice contains L sites in each direction, this amounts to setting up and diagonalizing an $L^4 \times L^4$ matrix, the complexity of which grows exponentially in L. At the same time, L determines the scale τ_{comp} at which boundary effects become dominant. To avoid fixed data on the boundary, we henceforth assume periodic boundary conditions, equipping the lattice with a toroidal topology. The resulting compactness leads to a falloff in spectral dimension for $\tau > \tau_{\text{comp}}$ [69]. Consequently, a large lattice size is required to observe a nontrivial spectral dimension between the smallest lattice scales $\tau \sim j_{\min}$ and τ_{comp}, which is in clear conflict with computational feasibility.

Apart from the computational effort to diagonalize the discrete Laplacian for a given spin configuration, the evaluation of the partition function becomes increasingly difficult with larger lattice size. That is because the number of spin configurations scales exponentially with the lattice sites. Because of spatial homogeneity there are in total $2L$ different spins, each of which takes $N = 2(j_{\max} - j_{\min}) + 1$ values. Here, $j_{\min}$ and $j_{\max}$ are the lower and upper cutoffs of the spins, respectively, the meaning of which we discuss in detail in Sec. IV A. Imposing the Riemannian EPRL condition of Eq. (2.2) and the inequality of Eq. (2.27), N allowed values for the spins (j_n, k_n) remain. The total number of configurations on the whole lattice is then N^{2L}. Consequently, the Laplacian needs to be diagonalized for each configuration to compute the return probability. This part is most demanding in numerical resources. Once the return probability for every spin configuration is obtained, the expectation value can be computed rather efficiently. To do so, one writes the amplitudes as a vector and the return probabilities as a matrix, with one index representing the configurations and the other one the diffusion time τ. The expectation value of the return probability is then obtained by a simple matrix-vector multiplication which is a highly optimized numerical operation.

To solve both of the above problems simultaneously, we adopt the assumption of $\mathcal{N}$ periodicity proposed in [13], based on the results of [71]. The key idea is to assume that the geometry of the spin foam is $\mathcal{N}$ periodic in every direction, meaning that the geometric labels repeat after $\mathcal{N}$ steps in every direction. As a consequence, one can perform a Fourier transform of the discrete Laplacian in the Brillouin zone which amounts to diagonalizing an $\mathcal{N}^4 \times \mathcal{N}^4$ matrix.

---

[10]Although simplifications for certain values of τ are conceivable, the viability of these would depend on the geometric configurations (j_n, k_n), obscuring a straightforward implementation.

The spectrum of the Laplacian is then given in terms of four momenta p_μ, which are either discrete or continuous, depending on whether the lattice is, respectively, finite or infinite. The return probability in Eq. (2.25) is then obtained as a sum and an integral, respectively, over the momenta. Also at the level of the amplitudes, periodicity reduces the computational complexity, as the number of independent spin variables reduces to $2\mathcal{N}$.

3. Spectrum of the discrete Laplacian

The first step in deriving the spectrum of the discrete Laplacian is to introduce the Fourier transform of the test field and to notice that the homogeneity of the geometry effectively reduces the Laplace coefficients $\Delta_{\vec{n}\vec{m}}$ to an $L \times L$ matrix. To make this explicit, let us first introduce some notation: We indicate the "spatial" component of $\vec{n} \in \mathbb{Z}_L^4$ as $\mathbf{n} \in \mathbb{Z}_L^3$. Taking $\mathcal{N}$ periodicity into account, we indicate a slice as $n_0 + z\mathcal{N}$ where $n_0 \in \mathbb{Z}_\mathcal{N}$ and $z \in \mathbb{Z}_{L/\mathcal{N}}$. Thus, the variable z labels the $\mathcal{N}$ cell in which the slice is located and n_0 denotes the n_0th slice within a given $\mathcal{N}$ cell. Using this notation, the scalar test field is written as $\phi_{n_0,\mathbf{n}}^{(z)}$ with $\phi_{n_0+\mathcal{N},\mathbf{n}}^{(z)} \equiv \phi_{n_0,\mathbf{n}}^{(z+1)}$.

To write Eq. (2.26) in Fourier space, we consider a similar ansatz to the proposal of [71], given by

$$\phi_{n_0,\mathbf{n}}^{(z)} = c_{n_0} e^{ip_0 z} e^{i\mathbf{n}\cdot\mathbf{p}}, \qquad (2.35)$$

where c_{n_0} is an $\mathcal{N}$-dimensional vector. A phase with spatial momentum p_i is picked whenever changing one lattice site in spatial direction i. In contrast, a phase with temporal momentum p_0 is only picked up when changing to another $\mathcal{N}$ cell. This pattern of picking up phases will be reflected in Eqs. (2.37)–(2.39). For a finite lattice of size L^4 with periodic boundary conditions, the momenta p_μ take values

$$p_\mu = \frac{2\pi}{L} k_\mu, \qquad k_\mu \in \mathbb{Z}_L. \qquad (2.36)$$

In the limit $L \to \infty$, the momenta lie in the Brillouin zone $p_\mu \in [-\pi, \pi]$. Inserting the ansatz of Eq. (2.35) into

Eq. (2.26), we obtain for $n \notin \{0, \mathcal{N} - 1\}$

$$-(\Delta c)_n = -\Big[\Delta_{nn+1}(c_n - c_{n+1}) + \Delta_{nn-1}(c_n - c_{n-1}) \\ + 2\Delta_{nn}c_n \sum_{i=1}^{3}(1 - \cos(p_i))\Big]. \qquad (2.37)$$

Δ_{nn+1} are the components of the Laplace operator on dual edges connecting slices n and $n + 1$, defined by Eqs. (2.28), (2.30), and (2.31). Δ_{nn} are the components of the Laplace operator within a slice, defined by Eqs. (2.28), (2.32), and (2.34), associated to spacelike separated vertices. Because of spatial homogeneity, Δ_{nn} is independent of the spatial direction and therefore factorizes from the spatial momenta. For the slices $n = 0, \mathcal{N} - 1$ connecting neighboring $\mathcal{N}$ cells, exponential factors of $e^{\pm ip_0}$ are picked up

$$-(\Delta c)_0 = -[w_0(c_0 - c_1) + w_{\mathcal{N}-1}(c_0 - c_{\mathcal{N}-1}e^{-ip_0}) + W_0 c_0], \qquad (2.38)$$

$$-(\Delta c)_{\mathcal{N}-1} = -[w_{\mathcal{N}-1}(c_{\mathcal{N}-1} - c_0 e^{ip_0}) \\ + w_{\mathcal{N}-2}(c_{\mathcal{N}-1} - c_{\mathcal{N}-2}) + W_{\mathcal{N}-1}c_{\mathcal{N}-1}], \qquad (2.39)$$

where for brevity, we introduced the notation

$$w_n := \Delta_{nn+1}, \qquad W_n := 2\Delta_{nn}\sum_i(1 - \cos(p_i)). \qquad (2.40)$$

Exploiting $\mathcal{N}$ periodicity and spatial homogeneity, we observe that the action of the Laplace operator reduces to a vector equation in $\mathcal{N}$ dimensions. Altogether, Eqs. (2.37)–(2.39) are captured by

$$-(\Delta c)_m = -\sum_{n=0}^{\mathcal{N}-1} M_{mn}c_n, \qquad (2.41)$$

with the matrix M being defined as

$$M := \begin{pmatrix} w_{\mathcal{N}-1} + w_0 + W_0 & -w_0 & \cdots & -w_{\mathcal{N}-1}e^{-ip_0} \\ -w_0 & w_0 + w_1 + W_1 & & \\ \vdots & & \ddots & \\ -w_{\mathcal{N}-1}e^{ip_0} & \cdots & -w_{\mathcal{N}-2} & w_{\mathcal{N}-2} + w_{\mathcal{N}-1} + W_{\mathcal{N}-1} \end{pmatrix}. \qquad (2.42)$$

For a given spin configuration, the spectrum in momentum space is then given by the eigenvalues of the matrix $M(p_0, p_1, p_2, p_3)$, which must be computed for every combination of momenta.

4. Expectation value of the return probability

Following Eq. (2.25), the return probability of a given spin configuration is obtained by either summing or integrating over the spectrum of the Laplacian. Let $\omega_i(\{p_\mu\})$

denote the $\mathcal{N}$ momentum-dependent eigenvalues of the Laplace matrix in Eq. (2.42). Then, the $\mathcal{N}$-periodic return probability $P_{\mathcal{N}}(\tau)$ on a lattice of length L is given by

$$P_{\mathcal{N}}(\tau) = \sum_{i=1}^{\mathcal{N}} \prod_{\mu=0}^{3} \sum_{k_\mu \in \mathbb{Z}_L} e^{-\tau\omega_i(\{p_\mu\})}, \qquad (2.43)$$

where the integers k_μ and the lattice momenta p_μ are related by Eq. (2.36). In the limit $L \to \infty$, the summation is replaced by an integration over the Brillouin zone, yielding

$$P_{\mathcal{N}}(\tau) = \sum_{i=1}^{\mathcal{N}} \prod_{\mu=0}^{3} \int_{-\pi}^{\pi} dp_\mu e^{-\tau\omega_i(\{p_\mu\})}. \qquad (2.44)$$

Notice, that the eigenvalues $\omega_i(\{p_\mu\})$ depend on the geometry of the entire lattice, turning the return probability into a highly nonlocal quantity. These different eigenvalues are usually called branches, e.g. the "acoustic" branch in which $\omega_i \to 0$ for all $p_\mu \to 0$.

Already for the two-periodic case, the summation and integration, respectively, in Eqs. (2.43) and (2.44) cannot be performed individually, since the eigenvalues $\omega_i(\{p_\mu\})$ do not split into a sum of terms for each momentum component p_μ. This severely affects the computational effort to compute the return probability at a given configuration. Summation is implemented by L^4 nested for-loops. For the numerical integration on the other hand, one cannot perform a product of one-dimensional integrals but needs to consider instead a single four-dimensional integration. Using the Cuba package,[11] such higher-dimensional integrations are possible but more costly and issues of convergence due to an exponential decay are more likely to arise.

The expectation value of the return probability for a finite $\mathcal{N}$-periodic lattice in this setting is

$$\langle P_{\mathcal{N}}(\tau) \rangle = \frac{1}{Z} \sum_{\{j_i,k_i\}} \left(\prod_{n=1}^{\mathcal{N}} \hat{\mathcal{A}}(j_n, j_{n+1}, k_n)^{L^3} \right)^{L/\mathcal{N}}$$
$$\times P_{\mathcal{N}}(\tau, \{j_i, k_i\}), \qquad (2.45)$$

where the spin labels are in the range $j_{\min} \leq j_i, k_i \leq j_{\max}$.[12] Note that *a priori*, $\mathcal{A}$ denotes the full quantum amplitude of four-frusta. However, as we argue in Sec. IV A, the asymptotics of the dressed vertex amplitude already captures the behavior of the spectral dimension sufficiently for $\tau \gtrsim 10^2$.

As argued in Sec. II B 2, the lattice size L is required to be large in order to resolve a nontrivial spectral dimension

---

between the minimal scale $\tau \sim j_{\min}$ and the compactness scale $\tau_{\text{comp}} \sim L$. Consequently, the amplitudes enter Eq. (2.45) with large powers, requiring the utilization of arbitrary precision floating point numbers. Arithmetics with this format are costly in memory and computation time. To circumvent this issue, we truncate the total number of amplitudes by assuming that the amplitudes of a single $\mathcal{N}$ cell sufficiently capture the relevant information of the whole spin foam. Within this approximation, the expectation value of the return probability is finally given by

$$\langle P_{\mathcal{N}}(\tau) \rangle = \frac{1}{Z} \sum_{\{j_i,k_i\}} \prod_{n=1}^{\mathcal{N}} \hat{\mathcal{A}}(j_n, j_{n+1}, k_n)^{\mathcal{N}^3} P_{\mathcal{N}}(\tau, \{j_i, k_i\}). \qquad (2.46)$$

In Sec. V B we discuss the limit of $\mathcal{N} \to \infty$, corresponding to an infinite lattice with infinitely many degrees of freedom.

To summarize, we compute the return probability for the spin foam quantum space-time by summing up the return probability for all possible spin foam frusta geometries, weighted by the quantum or semiclassical spin foam amplitudes $\hat{\mathcal{A}}$ for various diffusion times τ. From this expectation value, we derive the spectral dimension D_s as

$$D_S^{\mathcal{N}} := -2 \frac{\partial \ln\langle P_{\mathcal{N}}(\tau) \rangle}{\partial \ln \tau}. \qquad (2.47)$$

Notice, that we do not consider D_s as an observable itself. Rather, the "quantum spectral dimension" characterizes the *scaling* of a quantum expectation value, that is here the heat trace.

III. ONE-PERIODIC QUANTUM AMPLITUDES FROM EXTRAPOLATION

The quantum amplitudes of frusta spin foams, introduced in Sec. II A 1, are the necessary ingredients to determine expectation values. In essence, there are two ways to compute these. First, the intertwiners in Eq. (2.6) can be explicitly computed via SU(2) integrations. Then, as the formulas in Eqs. (2.4) and (2.5) suggest, quantum amplitudes are straightforwardly computed by contracting three-frustum and three-cube intertwiners accordingly. Notice, that due to the higher valence of the intertwiners, the frustum computation is more costly than an analogous computation on a triangulation. Another conceivable strategy is to derive a spin network expression of the vertex amplitude via SU(2)-recoupling theory, in the spirit of [34]. The result is then to be contracted with the overlap of intertwiners in the spin network and coherent state bases. Still in this case, the computation is more costly than in a triangulated setting.

Choosing to follow the first strategy, we face the following numerical challenge. Since the range of magnetic indices grows with the spin size, numerical

contractions of intertwiners either demand increasing memory when using the TensorOperations[13] package, or increasing time using nested for-loops. This sets numerical limits to the computation of the vertex amplitude already at low spins $j \sim 4$ [51], which is in conflict with resolving a nontrivial flow of the spectral dimension that requires $\frac{j_{\max}}{j_{\min}} \gg 1$, as argued below in Sec. IV A. Consequently, the number of configurations for which the exact quantum amplitudes are available, is insufficient to compute $\langle P(\tau) \rangle$.

While resorting to semiclassical amplitudes as done in [13] is a sensible choice, the approximation deviates significantly for small spins $j \lesssim 10$ [51]. In order to find amplitudes which are closer to the actual quantum amplitudes for small spins, while still showing a convergence to the semiclassical amplitudes in the limit of large spins, we present in this section a method to extrapolate quantum amplitudes in the simplest case of periodicity $\mathcal{N} = 1$ using the FindFit-function in *Mathematica* [72]. The restriction to one-periodic spin foam frusta reduces the model to a specific subclass of spin foam cuboids which satisfy geometricity [13,51,63]. A particular feature of cuboidal amplitudes is that they exhibit a pure scaling behavior without any oscillations, therefore simplifying the analysis drastically.

As mentioned above, the amplitudes of the Riemannian EPRL model factorize into SU(2) amplitudes for $\gamma_{\mathrm{BI}} < 1$. Thus, we first present an extrapolation method for the SU(2) vertex and edge amplitude in Sec. III A. Thereafter, we combine these results of that to set up an extrapolation of the dressed quantum vertex amplitude in Sec. III B, which will be used later on to compute the spectral dimension.

A. SU(2)-quantum amplitudes

One-periodic spin foam frusta are characterized by the amplitudes of a single four-frustum, the initial and final three-cubes of which carry the same spin j. The connecting three-frusta are uniquely characterized by the area of the trapezoidal faces, labeled by k. Hence, the pair (j, k) fully determines the geometry. In this case, the numerical limitations allow a computation of the exact quantum vertex and edge amplitudes for spins in the range $\frac{1}{2} \leq j, k \leq 4$ [51], thus yielding 64 data points.

Best suited for fitting, we compute the relative error

$$\varepsilon_i(j, k) := \frac{|\mathcal{A}_i^{\mathrm{sc}} - \mathcal{A}_i^{\mathrm{qu}}|}{\mathcal{A}_i^{\mathrm{sc}}} \qquad (3.1)$$

with respect to the semiclassical amplitudes, which are given in Eqs. (2.9) and (2.14). Here, i indicates the relative

error of vertex ($i = v$) and edge ($i = e$), respectively. Within a *homogeneous limit* ($\lambda j, \lambda k$) with $\lambda \to \infty$, the relative error ε_i converges to zero. Importantly, when keeping one variable fixed and only scaling the other one, we expect ε to converge to a small but nonzero value.[14] Still, this convergence will ensure that we obtain the convergence to the semiclassical amplitude in a homogeneous limit, as we demonstrate down below.

Now, for every j fixed, we find a fit of the relative error ε_i in the k direction. The resulting fitting function is then used to extrapolate ε_i up to a chosen value of $k = 5000$ for every j. With the results, we proceed similarly to extrapolate in j-direction for fixed k. Ultimately, we obtain a 10000×10000 matrix for the relative error $\varepsilon_i(j, k)$, from which the amplitudes can be derived via Eq. (3.1). Since the fitting procedure is only performed with one-dimensional functions, where either k or j is assumed to be fixed, it is a nontrivial consistency check to show the convergence of the quantum to the semiclassical amplitude in a homogeneous limit ($\lambda j, \lambda k$) with $\lambda \to \infty$. In the following, we show that this is indeed the case.

1. Extrapolated vertex amplitude

On the left panel of Fig. 6, we show that the relative error $\varepsilon_v(j, k)$ converges to zero in the limit where $(j, k) = (\lambda, \lambda)$ are homogeneously scaled up. For values of $\lambda \geq 13$, the relative error is smaller than 1%, as indicated by the black line in Fig. 6. Notice that we have plotted ε_v only up to $\lambda = 35$ since, from this value on, the difference between both amplitudes is already so small that it cannot be resolved with the usual double precision numbers. Notice that the two outlying points are a consequence of the fitting procedure and occur when there is a sign change in the fitting parameters. A side-by-side comparison of the extrapolated and semiclassical amplitude is presented on the right panel of Fig. 6. Clearly, the semiclassical amplitude is an overestimate of the extrapolated quantum amplitude for small spins which is alignment with the results of [13].

These results indicate that the extrapolated amplitude shows the correct behavior for large spins. Also for small spins, the extrapolated amplitude provides a better approximation of the actual quantum amplitude than the semiclassical. To show this explicitly, we present in Fig. 7 a plot of the relative error between the quantum amplitude and the extrapolated, semiclassical amplitude, respectively. When visible, the extrapolated amplitude is closer to the quantum amplitude by several orders of magnitude, measured by the relative error.

---

[13]See https://jutho.github.io/TensorOperations.jl/stable/ package for a documentation.

[14]Because of the restrictive nature of the frusta model in the one-periodic case, coupling rules are always satisfied. Furthermore, the boundary states are a function of the spins and at a critical point by construction.
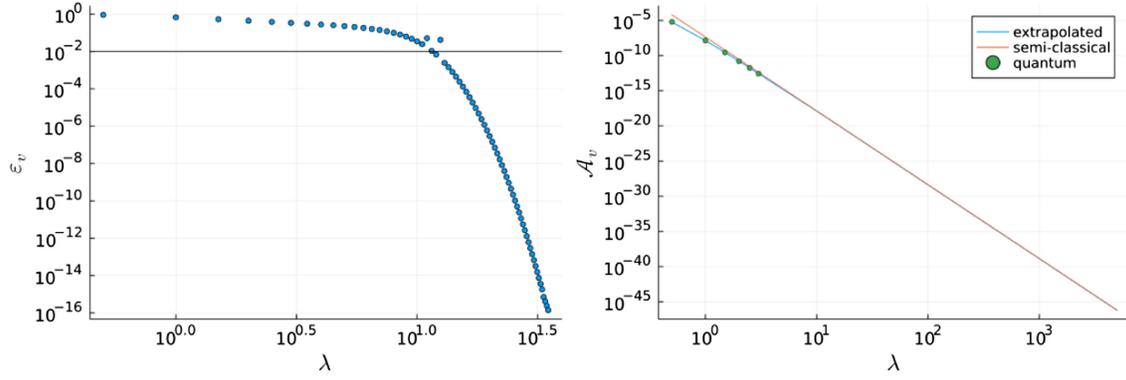
FIG. 6.   Left: Relative error ε_v between extrapolated and semiclassical SU(2)-vertex amplitude. Right: A direct comparison of the diagonal entries of the extrapolated, semiclassical and quantum SU(2)-vertex amplitude. We remind the reader that there are only a few quantum data points depicted since we are considering the diagonal case with $j = k$. For the fitting procedure, 64 data points have been utilized.
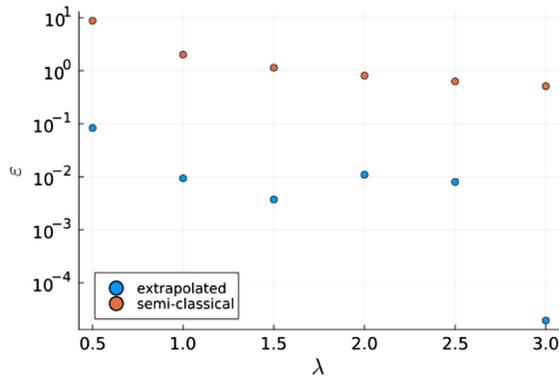
FIG. 7.   Relative error of the extrapolated and semiclassical vertex amplitude with respect to the exact SU(2)-quantum vertex amplitude.

2. Extrapolation edge amplitudes

The relative error ε_e between extrapolated quantum and semiclassical SU(2)-edge amplitudes is depicted on the left panel of Fig. 8. Similar to the vertex amplitude, we observe a rather fast convergence with $\varepsilon_e < 1\%$ at spins $\lambda > 13$. The plot is only drawn for $\lambda < 254$, since for larger spins, the difference between extrapolated and semiclassical amplitude cannot be resolved. On the right panel of Fig. 8, we see that the semiclassical edge amplitude underestimates the extrapolated amplitude for small spins. That is, because the edge amplitudes in Eq. (2.4) are defined as the inverse of the intertwiner norm.

Following this consistency check, we show in Fig. 9, that the extrapolated edge amplitude serves as a better estimate for the exact quantum amplitude at low spins. Indeed, the relative error between extrapolated and quantum amplitudes is below 1%, while it is of the order 1 for the semiclassical amplitude.

To summarize, the extrapolation of quantum amplitudes in the simplified case of one-periodic frusta spin foams provides a good approximation to the exact quantum amplitudes. For small spins in particular, the extrapolated amplitudes do not deviate as much from the quantum amplitudes in comparison to the semiclassical approximation. We emphasize that the whole procedure hinges on the assumption of one-periodicity. For higher periodicities
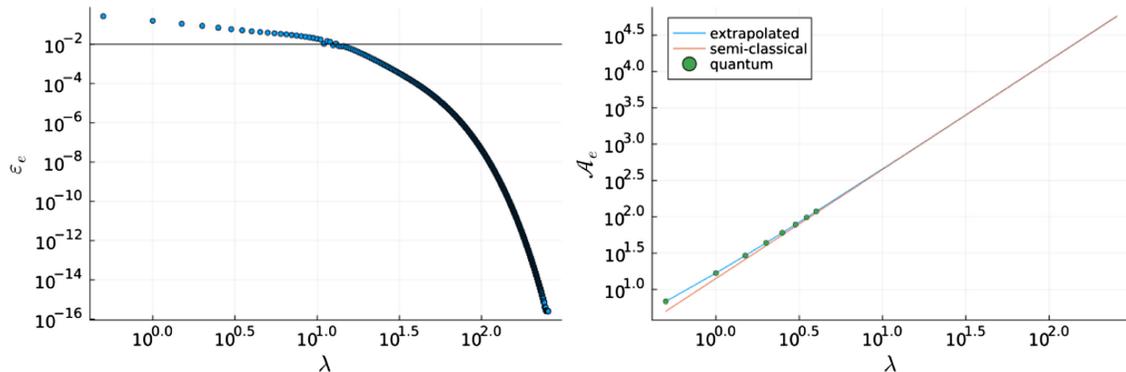
FIG. 8.   Left: Relative error ε_e between extrapolated and semiclassical SU(2)-edge amplitude. Right: A direct comparison of the diagonal entries of the extrapolated, semi-classical and quantum SU(2)-edge amplitude.
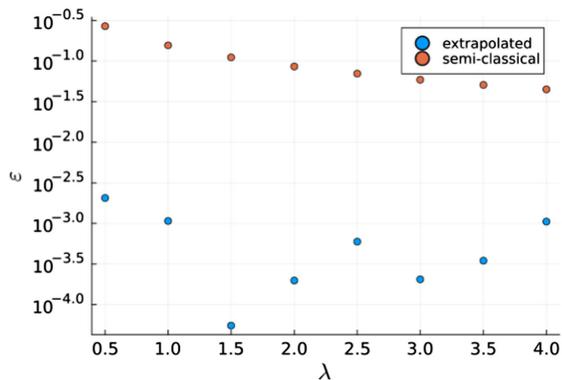
FIG. 9. Relative relative error of extrapolated and semiclassical edge amplitude with respect to the exact SU(2)-quantum edge amplitude.

FIG. 10. Relative error between extrapolated and semiclassical dressed amplitude, depending on $\alpha \in \{0.5, 0.75, 1.0\}$.

$\mathcal{N} > 1$, the vertex amplitudes oscillate. Since only few data points of the quantum amplitudes are available, it is to be expected that a simple fitting procedure cannot capture the behavior of the amplitudes sufficiently. To do so, one would probably have to assume the semiclassical oscillation behavior which, for small spins, yields the wrong phase [51]. Furthermore, this assumption might not be valid for a nonhomogeneous scaling, where all but one spin are kept fixed.

B. Dressed quantum vertex amplitude

In this section, we utilize the extrapolated SU(2) amplitudes of the previous section to compute an approximation of the quantum dressed vertex amplitude $\hat{\mathcal{A}}$ according to Eq. (2.16). Depending on the Barbero-Immirzi parameter γ_{BI}, the SU(2) spins j are mapped to different Spin(4) representations (j^+, j^-). Consequently, the components $\hat{\mathcal{A}}(j, j, k)$ are composed out of different components of SU(2) amplitudes $\mathcal{A}_i(j^\pm, j^\pm, k^\pm)$, where i indicates either face, edge, or vertex. Here and in the following section, we choose the least excluding value of $\gamma_{\mathrm{BI}} = \frac{1}{3}$ (see Fig. 1 for details) unless indicated otherwise. In this case $j \in \frac{3}{2}\mathbb{N}$ is mapped to $(\frac{2}{3}j, \frac{1}{3}j) \in \mathbb{N} \times \frac{1}{2}\mathbb{N}$, satisfying the EPRL condition in Eq. (2.2). We first analyze the convergence of the resulting amplitude to the semiclassical approximation in the limit $\lambda \to \infty$. Thereafter, we show that the extrapolated dressed vertex amplitude provides a better approximation than the semiclassical amplitude, which is to be expected from the results of Sec. III A. We conclude by presenting the effective scaling of the extrapolated dressed vertex amplitude, which is an important factor for the spectral dimension [13].

While the semiclassical SU(2) amplitudes provide a good approximation already at small spins of $\lambda \gtrsim 15$, the semiclassical Spin(4) amplitude is expected to have a slower convergence because of two reasons. First, since various powers of edge and vertex SU(2) amplitudes enter the
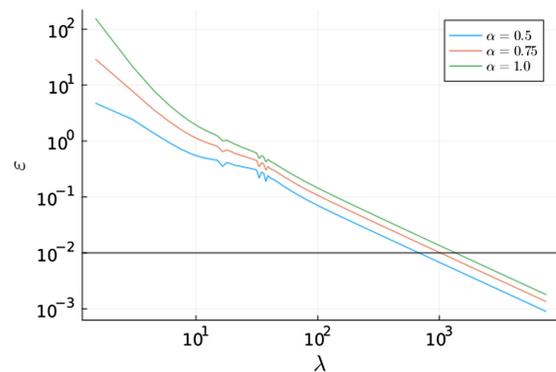
dressed amplitude, defined in Eq. (2.16), the relative errors ε_e and ε_v add up. Second, the face amplitude, given in Eq. (2.3), introduces a third deviation $\varepsilon_f(\alpha)$, which depends on the α parameter. By definition of the semiclassical and quantum face amplitude, a larger α leads to a stronger deviation. The plots of Fig. 10 support these arguments, where we consider the relative error between extrapolated and semiclassical amplitude for $\alpha \in \{0.5, 0.75, 1.0\}$. We find a good agreement of the two amplitudes for $\varepsilon < 1\%$, which is the case for spins $\lambda \sim 1000$.

To get a more detailed picture of its behavior and its dependence on α, Fig. 11 shows the extrapolated dressed amplitude in comparison to the semiclassical approximation for $\alpha \in \{0, 0.5, 0.75, 1.0\}$. Figure 11(a) depicts the dressed amplitudes for a trivial face amplitude. Here, the semiclassical amplitude is an overestimate for small spins. Increasing α to 0.5, which is a value of interest in Sec. IV, the extrapolated amplitude is in fact larger than the semiclassical one, as Fig. 11(b) shows. A short numerical check reveals that the transition from the amplitude being smaller to being larger than the semiclassical approximation takes place for $\alpha \lesssim 0.24$. At the value $\alpha = 0.75$, the semiclassical one-periodic amplitude becomes scale invariant. Following Fig. 11(c), the extrapolated dressed amplitude reaches the scale-invariant behavior asymptotically from above. Above scale invariance, the dressed amplitude diverges in the limit $\lambda \to \infty$. Visualized in Fig. 11(d), the extrapolated amplitude is larger than the semiclassical amplitude with a large relative error at small spins.

Only few components of the dressed Spin(4) amplitude can be computed, since the exact SU(2)-quantum vertex amplitude is only available for spins $j, k \leq 3$. Consequently, we can compute 3×3 entries of the exact dressed amplitude, listed in Fig. 12. There, the relative errors of extrapolated and semiclassical dressed amplitudes with respect to the exact quantum dressed amplitude are depicted for $\alpha = 0.5$. As indicated, the extrapolated dressed amplitude provides a better approximation to the quantum amplitudes for all tuples (j, k).
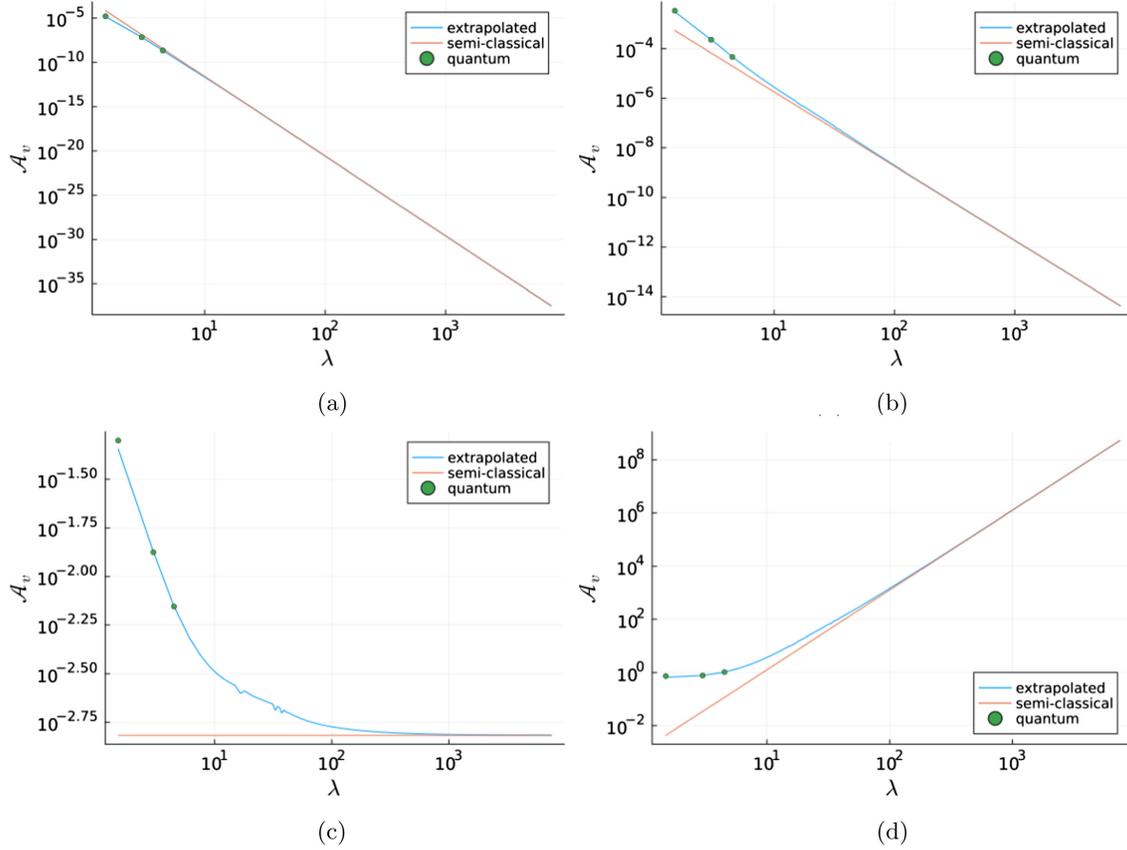
FIG. 11.   Comparison of extrapolated and semiclassical dressed vertex amplitudes for various values of α. (a) $\alpha = 0$, (b) $\alpha = 0.5$, (c) $\alpha = 0.75$, and (d) $\alpha = 1$.

As a last point, we compute the effective scaling γ of the extrapolated dressed amplitude, defined as

$$\gamma = -\frac{\lambda}{\hat{\mathcal{A}}} \frac{\partial \hat{\mathcal{A}}}{\partial \lambda}. \tag{3.2}$$
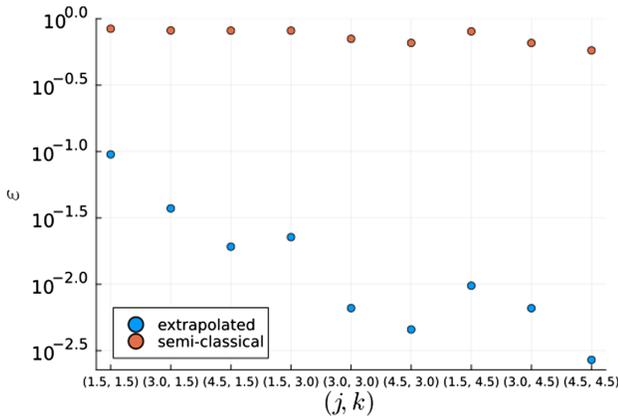
FIG. 12.   Relative error of extrapolated (blue) and semiclassical dressed vertex amplitudes with respect to the exact quantum dressed vertex amplitude. The values of ε are plotted against the tuple of spins (j, k) for which the exact quantum amplitude can be computed.

Demonstrated for cuboids in [13], the scaling of the amplitudes is a quintessential factor for the behavior of the spectral dimension. As we show later on in Sec. IV A and Sec. IV D, this holds also true for semiclassical as well as for extrapolated frusta amplitudes. A change in scaling directly translates to a change of the spectral dimension. Our results for the effective scalings with $\alpha \in \{0, 0.25, 0.5, 0.75, 1\}$ are presented in Fig. 13. For comparison, the semiclassical scaling exponents are depicted as black horizontal lines. These are constant because semiclassical amplitudes exhibit a simple polynomial decay. Since the extrapolated amplitudes approach the semiclassical limit from above for $\alpha > 0.24$, the corresponding effective scaling is below the constant semiclassical value. As expected from the previous arguments given above, exactly the opposite behavior can be observed for $\alpha = 0$.

IV. SPECTRAL DIMENSION FROM SPIN FOAM FRUSTA

With the ingredients introduced in Sec. II and Sec. III, we present in this section our numerical and analytical studies of the quantum spectral dimension for spin foam frusta. In Sec. IV A, we present numerical results using quantum and semiclassical one-periodic amplitudes. Proceeding with semiclassical amplitudes, we introduce a cosmological
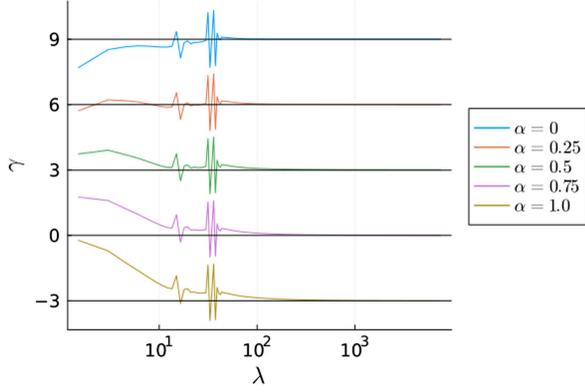
FIG. 13. Effective scaling behavior γ of the extrapolated dressed amplitude for $\alpha \in \{0, 0.25, 0.5, 0.75, 1\}$. Semiclassical constant values are indicated by the black lines. Fluctuations in the range $10^1 < \lambda < 10^2$ are due to numerical imprecisions in the fitting procedure, where the fitting parameters change sign.

constant in Sec. IV B and thereafter generalize to two-periodic configurations in Sec. IV C. We close this section with an analytical estimate of the spectral dimension in Sec. IV D.

A. One-periodic spectral dimension

Assuming that the geometry of frusta is one-periodic, the momentum space Laplace operator, defined in Eq. (2.42), reduces to a single component matrix

$$M = 2w_0(1 - \cos(p_0)) + W_0(p_1, p_2, p_3) = \sum_{\mu=0}^{3} \omega^{(\mu)}(p_\mu),$$
(4.1)

which decomposes into components $\omega^{(\mu)}(p_\mu)$. Consequently, the classical return probability on an infinite lattice, given in Eq. (2.44), can be written as a product of integrals
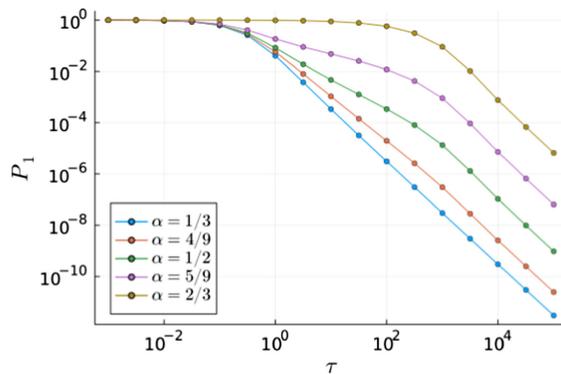
$$P_1(\tau) = \prod_{\mu=0}^{3} \int_{[-\pi,\pi]} dp_\mu e^{-\tau\omega^{(\mu)}(p_\mu)}$$

$$= \left(\int dp_0 e^{-\tau\omega^{(0)}(p_0)} \right) \left(\int dp_3 e^{-\tau\omega^{(3)}(p_3)} \right)^3, \quad (4.2)$$

where in the last step, we exploited spatial homogeneity. Factorization into one-dimensional integrals is advantageous, as the convergence of numerical integration impairs for increasing dimensionality.

Employing the extrapolated amplitudes of the previous section, we compute the expectation value of the return probability via Eq. (2.46). In the case of $\mathcal{N} = 1$, the formula reduces to

$$\langle P_1(\tau) \rangle = \frac{1}{Z} \sum_{j,k=j_{\min}}^{j_{\max}} \hat{\mathcal{A}}(j,j,k) P_1(\tau; j, k). \quad (4.3)$$

The numerical results for the expectation value of the return probability and the spectral dimension are presented in Fig. 14 for different values of α. Probing space-time at scales below the lowest lattice scale, $\tau \ll j_{\min}$, D_s is zero. Above the largest scale, i.e., $\tau \gg j_{\max}$, every classical configuration exhibits a spectral dimension of four and hence the quantum spectral dimension is four as well. Similar to the findings of [13], we observe a nontrivial dimensional flow between 0 and 4 for α in a certain interval $[\alpha_{\min}, \alpha_{\max}]$. We discuss in detail the various influence factors of the spectral dimension in the following paragraphs.

1. α parameter

The most salient factor driving the spectral dimension is the value of α. As Fig. 14 shows, only a small range of $\alpha \in [\alpha_{\min}, \alpha_{\max}]$ leads to an intermediate spectral dimension $D_s < D$. For any $\alpha < \alpha_{\min}$, the spectral dimension attains the value $D = 4$ without any nontrivial behavior before. Similarly, $\alpha > \alpha_{\max}$ suppresses an intermediate dimension $D_s \neq 0$ and D_s takes a finite nonzero value only at scales
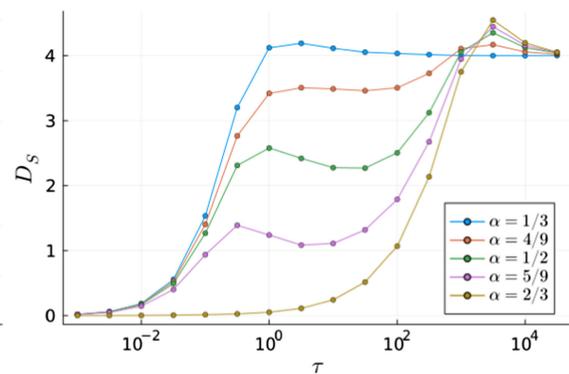
FIG. 14. Left: Expectation value of the one-periodic return probability. Right: Spectral dimension computed from the expectation value of the return probability. Both sets of data are computed with cut-offs $j_{\min} = \frac{1}{2}$ and $j_{\max} = 7500$.
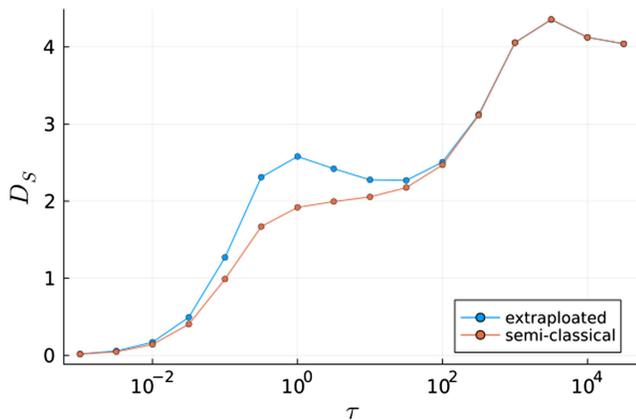
FIG. 15. Spectral dimension computed with extrapolated (blue) and semiclassical (red) amplitudes at $\alpha = 0.5$.

$\tau \gtrsim j_{\max}$. In Sec. IV D, we support the statements on the role of α with analytical considerations and present an estimate of the interval $[\alpha_{\min}, \alpha_{\max}]$.

2. Cutoffs

An intermediate spectral dimension between 0 and 4 is only resolved if the range of spins between $j_{\min}$ and $j_{\max}$ is sufficiently large. To be more precise, it is the ratio $\frac{j_{\max}}{j_{\min}}$ that is required to be sufficiently large. As numerical tests have shown, the ratio of cutoffs is required to be at least of order $\sim 10^2$ in order to resolve the first sign of a plateau. This signature in D_s presents itself as two points of inflection which are absent if less configurations are taken into account.

Because of the inherent minimal length scale in the theory, geometry cannot be probed below $\tau \sim j_{\min}$ such that this regime, where the spectral dimension flows to zero for $\tau \to 0$, is not of physical interest. Similarly, for scales $\tau \gg j_{\max}$, a dimension of four is inevitably reached, since all superimposed spin geometries possess a spectral dimension of four. While the existence of a minimal spin is a quintessential feature of most spin foam models, the upper cut-off is introduced for numerical purposes.[15] In order to recover a physical interpretation of our results, we therefore need to consider the limit $j_{\max} \to \infty$. As numerical tests with different $j_{\max}$ as well as the results of [13] show, the intermediate regime extends to infinity in the limit of infinitely large upper cut-off.

3. Barbero-Immirzi parameter

In the case of one-periodic spin foam frusta, the Barbero-Immirzi parameter γ_{BI} controls the spacing of allowed SU (2)-spins according to the $Y_{\gamma_{BI}}$ map defined in Eq. (2.2). Thus, changing the value of γ_{BI} results in a rescaling of the allowed spins, which in turn can be absorbed into the diffusion scale τ. This holds for quantum as well as for semiclassical amplitudes.[16] In contrast, the value of γ_{BI} has a nontrivial effect on amplitudes of $\mathcal{N} > 2$. As the semiclassical vertex amplitude in Eq. (2.13) suggests, γ_{BI} controls the relative phase of the oscillations. Therefore, it is, in general, to be expected that the spectral dimension is nontrivially affected by the value of γ_{BI}.

4 Compactness effects

Considering a finite lattice of length L with periodic boundary conditions rather than an infinite lattice, compactness effects are introduced to the spectral dimension which set in at scales $\tau > \tau_{\mathrm{comp}}(L)$.[17] Following [69], the return probability of a classical configuration with spins j is constant for $\tau > j$ and thus, the spectral dimension reaches zero at $\tau \sim j$. For the quantum spectral dimension, this implies that for L sufficiently large, i.e., such that $\tau_{\mathrm{comp}}(L) \gg j_{\max}$, a dimensional flow between zero, a possible intermediate value and four will be resolved. At τ close to compactness, D_s will then flow to zero and remain zero for all $\tau > \tau_{\mathrm{comp}}$. For $j_{\min} \lesssim \tau_{\mathrm{comp}} \lesssim j_{\max}$ and an intermediate regime D_s^α that is existent, the spectral dimension will flow to this intermediate value and then back to zero after the compactness scale is reached. For $\tau_{\mathrm{comp}} \ll j_{\min}$, the spectral dimension is zero everywhere.

5 Semiclassical amplitudes

Employing the semiclassical amplitude for computing the expectation value of the return probability and the spectral dimension, we observe a behavior similar to that obtained with extrapolated amplitudes. A direct comparison is presented in Fig. 15 for $\alpha = 0.5$. With semiclassical amplitudes, the spectral dimension is constant in the intermediate regime. In particular, in the limit $j_{\max} \to \infty$, where the upper cutoff is removed, this plateau extends to $\tau \to \infty$.

Considering the results of Sec. III B and the analytical explanations of [13], the deviation between the two curves is a consequence of the different scaling behaviors of the

---

[15]Following [66,67,73], apart from what is considered in this work, a cosmological constant can be added to spin foams by replacing the group SU(2) by its quantum deformation SU(2)$_q$. Consequently, an upper cutoff $j_{\max}$ is introduced, related to the cosmological constant via $j_{\max} \sim \frac{\pi}{\Lambda l_P^2}$ [64]. However, this value is expected to be much larger than what can could numerically implemented. For instance, a cosmological constant of order $\sim 10^{-122}$ would imply a maximal cutoff of order $j_{\max} \sim 10^{122}$.

[16]For $j \in \mathbb{N}/2$ that do not satisfy the EPRL condition, the amplitudes are zero. We exploit this exclusion for the computation of the return probability in that we only compute it for the allowed configurations, given a value of γ_{BI}. All other components would be multiplied with zero in the expectation value.

[17]For a comparison to the continuum spectral dimension of a torus, we refer to [26], where the compactness effects are clearly visible.

amplitudes for small spins. From Fig. 13, it follows that larger effective inverse scaling γ of the amplitudes implies a larger spectral dimension. Also, since the effective scaling of the extrapolated amplitudes is nonconstant, there is a nonconstant flow of the spectral dimension to the semi-classical constant value at larger scales.[18] As this flow is visible at scales $\tau > 10$, it is not a mere discreteness artifact but a physical effect.

The different behavior of the spectral dimension due to the different amplitudes appears in the regime $10^{-2} < \tau < 10^2$ and is of quantitative nature. Although providing an increasingly bad approximation at low spins, this suggests that the semiclassical amplitude is sufficient for extracting the spectral dimension on large scales. In particular, there is agreement with the quantum amplitude results for scales $\tau > 10^2$, even in the limit of infinite upper cutoff. Therefore, we are going to employ semiclassical amplitudes for the rest of this work.

Using the semiclassical amplitudes comes with the following three advantages. First, having an analytical expression for the amplitudes available allows for numerical integration, which is based on assuming the spins to be continuous variables. In that way, the results we have obtained so far can be compared to the findings of [13], which are based on continuous integration. Second, the semiclassical setting allows for a straightforward inclusion of a cosmological constant via an *ad hoc* deformation of the amplitudes [66,67]. Third, the extrapolation method for quantum amplitudes, discussed in Sec. III, strongly relies on the assumption of one-periodicity. Since we do not expect this method to be straightforwardly applicable for $\mathcal{N} > 1$, quantum amplitudes beyond small spins are not in reach for $\mathcal{N} > 1$. Because of these technical limitations, resorting to semiclassical amplitudes allows the study of the spectral dimension at higher periodicities. In the following, we take advantage of the possibilities that the semiclassical amplitudes offer, and discuss these cases in greater detail.

6 Discrete summation vs numerical integration

Up to this point, we computed the expectation value of the return probability via a discrete sum over all spin configurations in the range $j_{\min} \leq j, k \leq j_{\max}$. In the case where $\frac{j_{\max}}{j_{\min}} \gg 1$, the sum can be replaced by an integral, which is the strategy employed in [13]. As a consequence, the expectation value of the return probability is obtained as an integral over the configurations with the amplitudes and the return probability being continuous functions of the spins. Note that, for this strategy, an analytical expression of the amplitudes is required. Determining the corresponding functions for quantum amplitudes is currently out of

reach. Therefore, one needs to resort to the semi-classical approximation, where the spins are simply understood as continuous variables.[19] We have numerically checked that both methods yield very similar results. For small and large τ, we observe a convergence, while the spectral dimension differs quantitatively in the regime where the intermediate value D_S^α is reached. This is, because according to [69], continuous configuration variables lead to a smoothening of discreteness peaks.

B. Cosmological constant

A way to add a cosmological constant to the simplicial EPRL-FK model was introduced in [66] and generalized to arbitrary four-dimensional polyhedra in [67]. In essence, the vertex amplitudes of the model are deformed while keeping the boundary Hilbert space fixed. Relating the deformation parameter with the cosmological constant, the asymptotic vertex amplitude yields the Regge action with a cosmological constant.[20] Given that the Regge curvature, defined in Eq. (2.12), vanishes for one-periodic configurations, the introduction of a cosmological constant allows us to consider oscillations even when $\mathcal{N} = 1$. In this setting, the sign of the cosmological constant is irrelevant for the amplitudes, as Eq. (4.4) below shows. Following from the definition of the Spin(4)-vertex amplitude defined in Eq. (2.13), these oscillations are of a particular type in comparison to cases of vanishing Regge curvature. First, Λ oscillations allow only for simple cosine type shape. In contrast, the Regge term describes a superposition of cosines with different phases controlled by the Barbero-Immirzi parameter. Notice that this superposition is a peculiar feature of the Riemannian EPRL model, which is absent in the Lorentzian setting [33]. Second, since Λ enters the action via a four-volume, these oscillations scale quadratically in spins, whereas curvature terms scale linearly. Despite its simple form, we consider the cosmological constant in order to get a first glimpse of the effects of oscillations on the spectral dimension.

Explicitly, the oscillating term is given by

$$\cos\left(\frac{\Lambda}{G} jk\right) - \frac{\mathfrak{Re}\{D\}}{|D|}, \qquad (4.4)$$

where D is the determinant of the Hessian, defined in Eq. (2.10). Consequently, for a given upper cutoff $j_{\max}$, the amplitudes and hence the return probability are not altered

---

[18]This effect is only partially resolved in Fig. 15, since effects of the upper cutoff appear for large τ.

[19]Notice, that the EPRL condition of Eq. (2.2) cannot be implemented, since it would yield a function of measure zero.

[20]Another mathematically more rigorous way of introducing a cosmological constant to spin foams is to replace the group SU(2) by its quantum deformation $SU(2)_q$ [73–79]. The deformation parameter q is related to Λ via $q = \exp(2\pi i/(k + 2))$ with $k = 1/(\hbar G \sqrt{\Lambda})$; see, e.g., [77]. For more methods on implementing a cosmological constant in 4D spin foams see, e.g., [80,81].
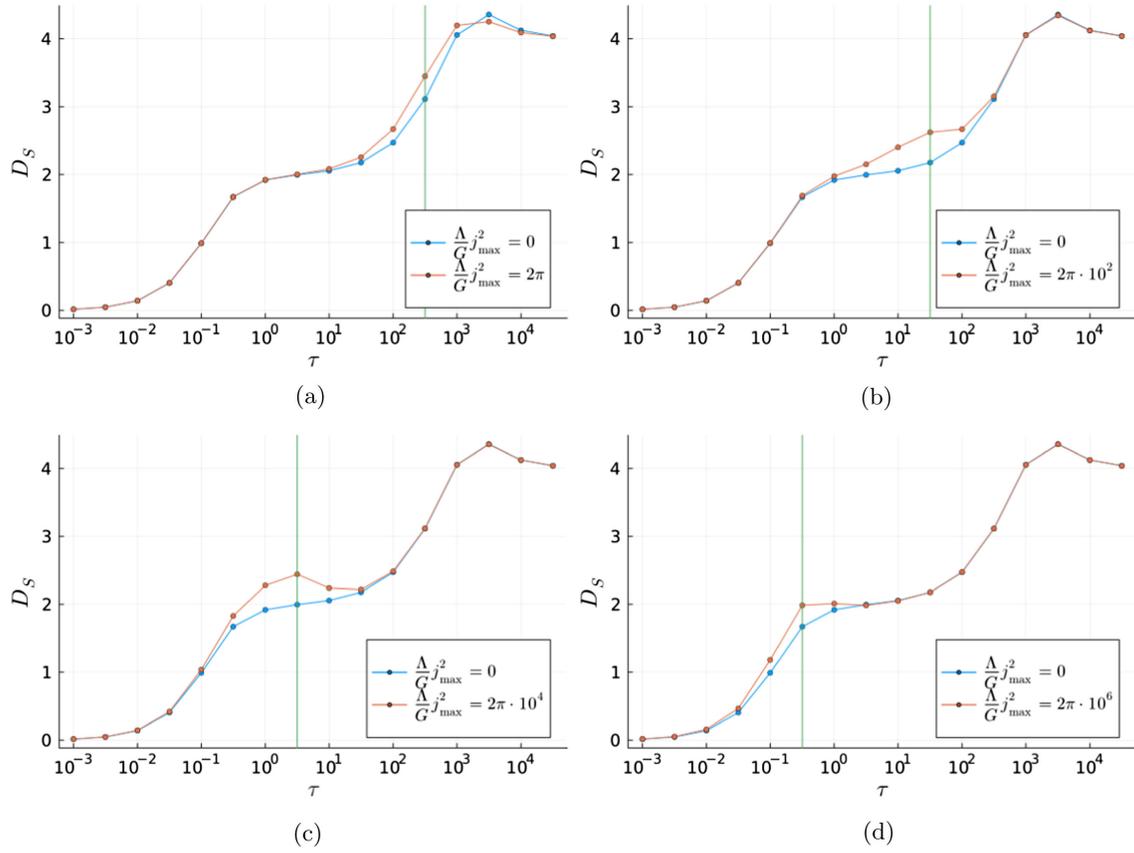
FIG. 16. Spectral dimension at $\alpha = 0.5$ with different values of the cosmological constant $\Lambda - G$. Notice that, in general, the values of Λ are independent of $j_{\max}$. (a) $\frac{\Lambda}{G} j_{\max}^2 = 2\pi$, (b) $\frac{\Lambda}{G} j_{\max}^2 = 2\pi 10^2$, (c) $\frac{\Lambda}{G} j_{\max}^2 = 2\pi 10^4$, and (d) $\frac{\Lambda}{G} j_{\max}^2 = 2\pi 10^6$.

for $\frac{\Lambda}{G} \ll \frac{1}{j_{\max}^2}$ since the argument of the cosine is small for all possible values of spins. However, for $\frac{\Lambda}{G} \gtrsim \frac{1}{j_{\max}^2}$ the spectral dimension is affected by the oscillations of the amplitudes, as Fig. 16 shows.

The strongest deviation from the $\Lambda = 0$ case is localized at the scale at which the first oscillation takes place, marked by a green vertical line. If this scale is in the intermediate regime, the spectral dimension is larger than in the case of vanishing Λ. To be more precise, it is the regime below the first zero of the amplitudes, given by

$$\lambda_0^{(\Lambda)} = \sqrt{\frac{G}{\Lambda} \arccos\left(\frac{\mathfrak{Re}\{D\}}{|D|}\right)} \qquad (4.5)$$
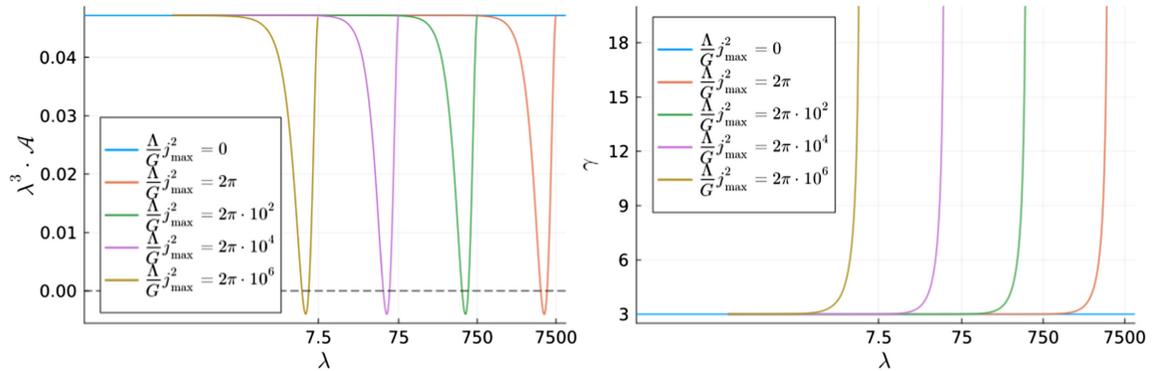
FIG. 17. Left: The first complete oscillation of the rescaled amplitudes for different values of Λ/G, given $\alpha = 0.5$. The dashed line indicates zero, which is crossed for the first time at $\lambda = \lambda_0^{(\Lambda)}$. Right: Scaling γ of the amplitudes for $\lambda < \lambda_0^{(\Lambda)}$ with the same parameters as on the left. Notice that both of the plots assume the spin variable λ to be continuous, ignoring the EPRL condition.

which we expect to be most influential. To visualize this, Fig. 17 shows the first oscillation of the (rescaled) amplitudes as well as the effective scaling γ of the amplitude for all $\lambda < \lambda_0^{(\Lambda)}$. Since the shift in Eq. (4.4) is constant, the oscillations are not symmetric with respect to the λ axis. Still, since $\left|\frac{\Re\{D\}}{|D|}\right| < 1$, the amplitudes attain negative values when crossing zero, indicated by the dashed line. The zeros as well as the extrema of the amplitudes lead to an abrupt change in sign of the scaling γ. Consequently, for $\lambda > \lambda_0^{(\Lambda)}$, the scaling oscillates rapidly, which, however, does not affect the spectral dimension. Similar to the comparison of quantum and semi-classical amplitudes, a value $\gamma > 9 - 12\alpha$ larger than the semiclassical scaling implies a larger spectral dimension. This effect is, in particular, resolved in the regime $\lambda < \lambda_0^{(\Lambda)}$. Notice that an increase of D_s is a feature present for all values of $\Lambda \neq 0$, since the amplitudes exhibit a scaling $\gamma > 9 - 12\alpha$ for $\lambda < \lambda_0^{(\Lambda)}$.

C. Two-periodic spectral dimension

The results of the previous section have shown that the semiclassical amplitude serves as a sufficient approximation to extract the qualitative behavior of the spectral dimension in the one-periodic case. It is therefore reasonable to employ the semiclassical amplitudes to compute the spectral dimension with higher periodicity, which are $\mathcal{N} = 2$ here. We discuss possible quantum corrections to our results at the end of this section.

Following Eq. (2.42), the Laplace operator at $\mathcal{N} = 2$ becomes a 2×2 matrix in momentum space

$$M = \begin{pmatrix} w_0 + w_1 + W_0 & -w_0 - w_1 e^{-ip_0} \\ -w_0 - w_1 e^{ip_0} & w_0 + w_1 + W_1 \end{pmatrix}, \quad (4.6)$$

where W_0 and W_1, defined in Eq. (2.40), depend on the spatial momenta p_i. The corresponding eigenvalues are given by

$$\omega_\pm(p_\mu) = w_0 + w_1 + \frac{W_0 + W_1}{2} \\ \pm \sqrt{w_0^2 + w_1^2 + 2w_0 w_1 \cos(p_0) + \left(\frac{W_0 - W_1}{2}\right)^2}.$$

$$(4.7)$$

Compared to the one-periodic case in Eq. (4.2), this expression is more involved due to the intermingling of the p_0 and p_i terms. As a consequence, the return probability from momentum integration,

$$P_2(\tau) = \sum_{\epsilon = \pm} \int \prod_{\mu=0}^{3} \mathrm{d}p_\mu e^{-\tau \omega_\epsilon(\{p_\nu\})}, \quad (4.8)$$

cannot be written as the product of one-dimensional integrals. Instead, full four-dimensional integration is required to compute P_2, leading to larger numerical computation times.

Under the assumption that the amplitudes of a single $\mathcal{N}$ cell, here a two-cell consisting of 16 hyperfrusta, already capture the relevant information, the full expression for the expectation value of the return probability is given by

$$\langle P_2(\tau) \rangle = \frac{1}{Z} \sum_{j_1, j_2, k_1, k_2} (\hat{\mathcal{A}}(j_1, j_2, k_1))^8 (\hat{\mathcal{A}}(j_2, j_1, k_2))^8 \\ \times P_2(\tau; j_1, j_2, k_1, k_2). \quad (4.9)$$

Again, the range of all of the spins is given by $j_{\min} \leq j_i$, $k_i \leq j_{\max}$. For the numerical results presented below, we have chosen $j_{\min} = \frac{1}{2}$ and $j_{\max} = 201$. Since in the two-periodic case, the three-cubes are not restricted to equal size, frustum geometries arise which lead to nonvanishing Regge curvature. Consequently, the vertex amplitudes $\hat{\mathcal{A}}$ exhibit oscillations even in the case of a vanishing cosmological constant, $\Lambda = 0$, which we assume from now on if not stated otherwise. Given three fixed spins (j, j', k), a single dressed vertex amplitude scales as

$$\hat{\mathcal{A}}(\lambda j, \lambda j', \lambda k) \sim \lambda^{12\alpha - 9} \left[\cos\left(\frac{\gamma_{\mathrm{BI}}}{G} \lambda S_R(j, j', k)\right) \\ - \cos\left(\frac{1}{G} \lambda S_R(j, j', k) - \varphi(j, j', k)\right) \right], \quad (4.10)$$

where S_R is the Regge action and φ is the phase of the determinant D of the Hessian, both being evaluated on the spins (j, j', k). Notice that φ is invariant under a homogeneous scaling of all spins. Since the expectation value of the two-periodic return probability, Eq. (4.9), contains high powers of cosine functions, the amplitudes are narrowly peaked on the maxima of oscillation. Furthermore, since the powers in Eq. (4.9) are even, no negative values occur.

1. Large Newton's constant

As a first computation, we consider the limiting case of $G \to \infty$, where curvature oscillations become negligible. In Fig. 18 we present the results for $G = 10^{10}$. This already captures the large G behavior for the chosen $j_{\max}$ as we have checked that for larger G the results do not change anymore.

Just as for the one-periodic case, we observe that there exists an intermediate flow of the spectral dimension for α values in a certain interval $\alpha \in [\alpha_{\min}, \alpha_{\max}]$, where $\alpha_{\min} \approx 0.68$ and $\alpha_{\max} \approx 0.7$. From the results Sec. IV A, we conclude that the intermediate spectral dimension is again a result of the amplitudes exhibiting a scaling behavior. Compared to the one-periodic case, the size of the interval of α is smaller which is in accordance with the findings
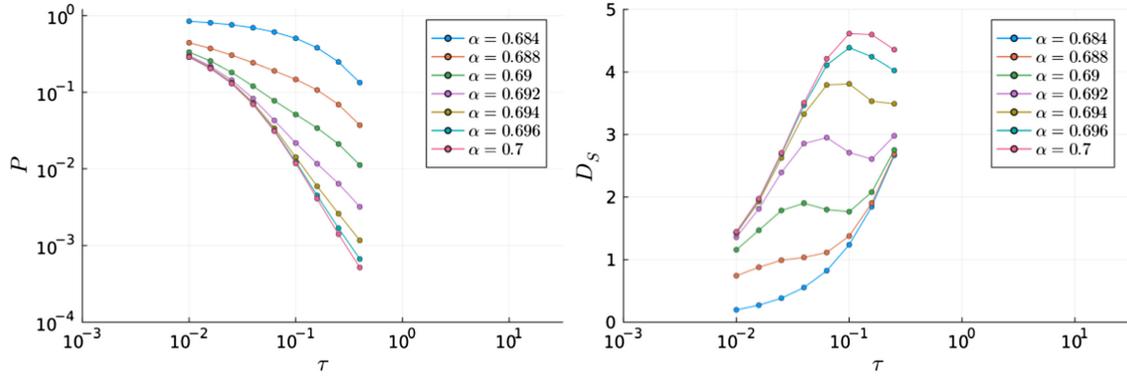
FIG. 18. Left: Expectation value of the two-periodic return probability. Right: Two-periodic spectral dimension. Parameters G, γ_{BI}, and Λ are set to $G = 10^{10}$, $\gamma_{BI} = 1/3$, and $\Lambda = 0$ with cutoffs $j_{min} = 1/2$ and $j_{max} = 201$.

of [13]. As we are going to discuss in more detail in Sec. IV D, this is expected. In the following we discuss the effects of a finite value of G.

2. Regge curvature oscillations

Given that, in principle, an intermediate spectral dimension D_s^α can be observed in the case of $\mathcal{N} = 2$, we study next the influence of oscillating amplitudes by varying G. Following from the form of the amplitudes in Eq. (4.10), Regge curvature oscillations are expected to become relevant for G being comparable to S_R. In the light of the results of Sec. IV B, we expect that the oscillations, now induced by Regge curvature, have an effect on the spectral dimension. Our numerical results show that the spectral dimension is indeed perceptive to the value of G. Since small changes in G lead to very different flows of D_s, we conclude that the spectral dimension is in fact highly sensitive to Newton's constant. In Fig. 19, we present the spectral dimension at fixed α for three exemplary values of G, showing that one can have either a positive or a negative correction to the case $G \to \infty$, or no correction at all.
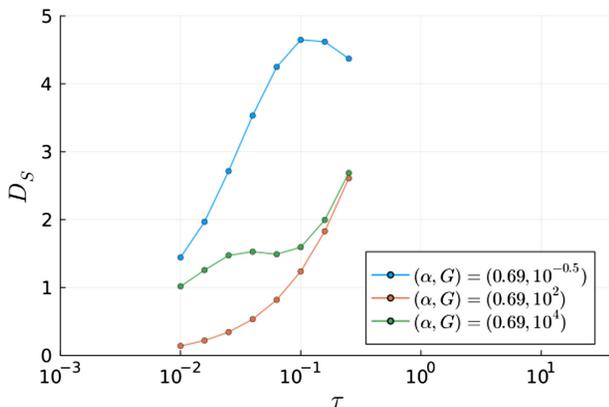
FIG. 19. Two-periodic spectral dimension at $\alpha = 0.69$ for three exemplary values of G.

In contrast to one-periodic amplitudes oscillating with a cosmological constant, the flow of the two-periodic spectral dimension is not straightforwardly understood by considering the scaling behavior of the amplitudes. The main reason for that is the strong dependence of the amplitudes on the spins (j, j', k), given explicitly in Eq. (4.10).

3. G-dependence of intermediate regime

Given the plots of Fig. 19, the blue and red curves might indicate that the interval $[\alpha_{min}, \alpha_{max}]$ in which an intermediate spectral dimension occurs depends on the value of G. We test this possibility by computing the spectral dimension for $G = 10^{-0.5}$ and $G = 10^2$ and a wide range of α. Our results are depicted in Fig. 20. Indeed, we observe that for different values of G the boundaries α_{min} and α_{max} change. While at $G = 10^{-0.5}$, these are $\alpha_{min} \approx 0.67$ and $\alpha_{max} \approx 0.69$, their values at $G = 10^2$ are $\alpha_{min} \approx 0.69$ and $\alpha_{max} \approx 0.71$.

An additional feature we observe is the following. Within the interval $[\alpha_{min}, \alpha_{max}]$, the spectral dimension of purely scaling amplitudes is approximately a decreasing linear function of α. In contrast, Fig. 20 suggests that the slope of D_s as a function of α can be positive or negative, depending on G. We will discuss interpretations of these phenomena and their entailing consequences for the limit of large periodicities $\mathcal{N}$ in Sec. V B.

4. Cosmological constant

Since the Regge curvature does not vanish for $\mathcal{N} > 1$, the effects of a nonvanishing cosmological constant, $\Lambda \neq 0$, on the amplitudes is not as apparent as in the one-periodic case. Following Eq. (2.13), Λ introduces a phase shift to the cosine term containing the parameter γ_{BI}. Entering with the four-volume of the frusta, such a term scales quadratically in the spins, leading to an intricate behavior in combination with the Regge curvature contributions. Fixing $G = 1$ and $\alpha = 0.69$, we present the two-periodic spectral dimension for a selection of Λ-values in Fig. 21.
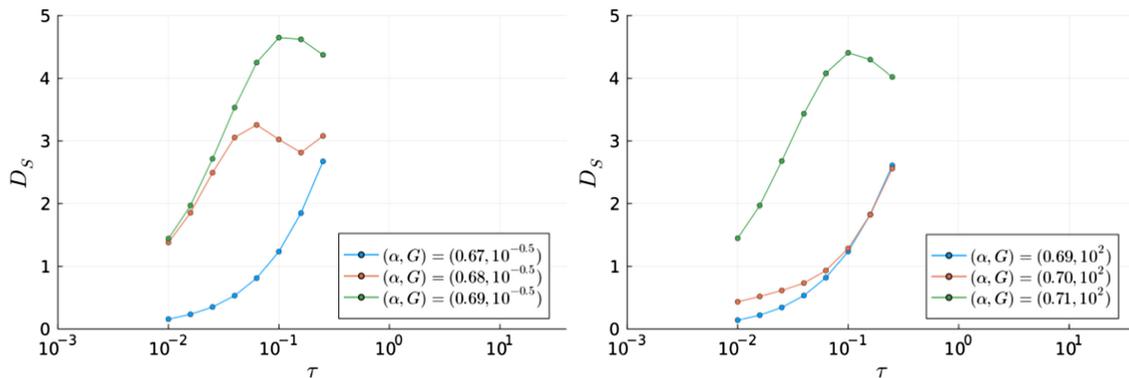
FIG. 20. Two-periodic spectral dimension for $G = 10^{-0.5}$ (left) and $G = 10^2$ (right) showing that the window of an intermediate regime is G-dependent.
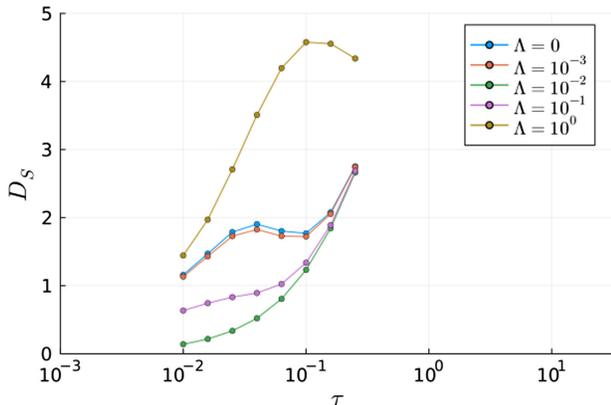
FIG. 21. Two-periodic spectral dimension for varying Λ, with $G = 1$ and $\alpha = 0.69$.

Effects of Λ become important only for Λ when it is not much smaller than G, as expected from the form of the amplitudes. The resulting phase shift in the oscillating part of the amplitudes has significant impact on the flow of the spectral dimension, as Fig. 21 shows. In comparison to the one-periodic case discussed in Sec. IV B, we observe the following additional features. First, high frequency oscillations due to large values of Λ do not appear negligible, at least in the small range of τ that we can observe. Second, the region of τ's, where Λ leads to a deviation in the flow of D_{s}, is not as clearly localized as in Fig. 16. This is apparent by observing that in the region $\tau \in [10^{-2}, 10^{-0.6}]$, the spectral dimension is affected for various orders of magnitude of Λ. Third, the direction in which the spectral dimension is corrected by the presence of Λ, so to lower or larger values than for $\Lambda = 0$, is obscured compared to the one-periodic case. That is, because Λ does not solely control the position of the first root of the amplitudes when $\mathcal{N} = 2$ but leads to a phase shift, the consequences of which are not as straightforward to analyze.

In the presence of a nonvanishing Regge curvature, the amplitudes are not invariant under a sign change of Λ. However, numerical tests have shown that, at least for

the small region of τ's depicted in Fig. 21, different signs of Λ have a negligible effect in D_{s}^{α}. Hence, the magnitude of the cosmological constant appears to be the significant quantity.

Similar to the above, we find that the range of α, for which an intermediate dimension exists, depends on the value of Λ. In summary, α_{min} and α_{max} are functions of both Newton's constant G as well as the cosmological constant Λ. We will pursue this discussion in Sec. V B.

D. Analytical estimate of the spectral dimension

Building up on the ideas of [13], we present in this section a strategy to extract information from the spectral dimension of oscillating amplitudes using analytical methods. Tackling first the spectral dimension of general $\mathcal{N}$-periodic spin foam frusta, we obtain a qualitative expression for the spectral dimension which is, however, still too intricate to compute explicitly. Nevertheless it serves as a support for the numerical results as well as a guidance for the limit $\mathcal{N} \to \infty$, discussed in Sec. V B. In the second part of this section, we consider an explicitly integrable model which qualitatively explains the cosmological constant results of Sec. IV B.

1. An analytical argument

For the analysis of the spectral dimension, it is advantageous to introduce the average spin variable $r^2 := \frac{1}{n} \sum j_f^2$, where n is the total number of degrees of freedom, where $n = 2\mathcal{N}$ in the case of $\mathcal{N}$-periodic spin foam frusta. Technically, the variable r is a radial coordinate in the space of configurations j_f. Likewise, the remaining variables can be seen as an angular part, and we therefore denote them by Ω in the following. As the definition of the Laplace operator in Sec. II B 1 and the arguments of [71] and [13,27] show, it is reasonable to assume under the spin foam measure

$$\Delta(j_f) \sim \frac{1}{r} \Delta, \qquad (4.11)$$

where Δ is the Laplace matrix on the equilateral hypercubic lattice.

Within this assumption, let us have a closer look on the expectation value of the return probability with respect to semiclassical amplitudes. As we have argued in Sec. IV A, for $\frac{j_{\max}}{j_{\min}} \gg 1$, the summation over configurations can be approximated by an integral. Following that and performing a change to spherical coordinates as described above, we obtain

$$\langle P(\tau) \rangle = \frac{1}{Z} \int d\Omega \int_{j_{\min}}^{j_{\max}} dr r^{n-1} \prod_v \mathcal{A}_v(r, \Omega) \mathrm{Tr}(e^{\frac{\tau\Delta}{r}}). \quad (4.12)$$

Forming the logarithmic derivative of this expression yields

$$\frac{\tau}{\langle P \rangle} \frac{\partial \langle P \rangle}{\partial \tau} = \frac{1}{\langle P \rangle Z} \int dr d\Omega r^{n-1} \prod_v \mathcal{A}_v \mathrm{Tr}\left(\frac{\tau\Delta}{r} e^{\frac{\tau\Delta}{r}}\right). \quad (4.13)$$

Since $\mathrm{Tr}(e^{\frac{\tau\Delta}{r}})$ is in fact a function of the ratio τ/r, we can trade the derivative with respect to τ with an r derivative,

$$\mathrm{Tr}\left(\frac{\tau\Delta}{r} e^{\frac{\tau\Delta}{r}}\right) = -r \frac{\partial}{\partial r} \mathrm{Tr}(e^{\frac{\tau\Delta}{r}}). \quad (4.14)$$

Using the r derivative, we can integrate by parts,

$$\frac{\tau}{\langle P \rangle} \frac{\partial \langle P \rangle}{\partial \tau} = \frac{1}{\langle P \rangle Z} \left[\partial I(\tau) + \int dr d\Omega r^{n-1} \prod_v \mathcal{A}_v \right.$$
$$\left. \times \left(n + \sum_v \frac{r}{\mathcal{A}_v} \frac{\partial \mathcal{A}_v}{\partial r} \right) \mathrm{Tr}(e^{\frac{\tau\Delta}{r}}) \right]. \quad (4.15)$$

Here, ∂I denotes the boundary term in the partial integration, explicitly given by

$$\partial I(\tau) = -\int d\Omega r^n \prod_v \mathcal{A}_v \mathrm{Tr}(e^{\frac{\tau\Delta}{r}})|_{r=j_{\min}}^{j_{\max}}. \quad (4.16)$$

The other terms inside the brackets stem from the r derivative acting first on r^n and then on the product of amplitudes. Notice that $-\frac{r}{\mathcal{A}_v} \frac{\partial \mathcal{A}_v}{\partial r}$ is exactly the effective scaling γ of $\mathcal{A}_v$ which we have discussed previously in Sec. III B.

Before tackling more general cases, we consider the simplified scenario in which the amplitudes satisfy a uniform scaling behavior, i.e., $\mathcal{A}_v = h_v(\Omega) r^{-\gamma_{\mathrm{cons}}}$. For a scaling $\gamma_{\mathrm{cons}} = 9\text{--}12\alpha$, this describes $\mathcal{N}$-periodic cuboids (and thus one-periodic frusta) with a vanishing cosmological constant, $\Lambda = 0$. Importantly, the radial and angular parts factorize as a consequence of the scaling assumption of Δ, simplifying the following equations significantly. As the effective scaling of $\mathcal{A}_v$ with respect to the radial coordinate is the constant γ_{cons}, the spectral dimension is

$$D_{\mathrm{s}}(\tau) = -2 \frac{\tau}{\langle P \rangle} \frac{\partial \langle P \rangle}{\partial \tau} = 2(\gamma_{\mathrm{cons}} V - n) - 2 \frac{\partial I(\tau)}{\langle P \rangle Z}. \quad (4.17)$$

Our results from one-periodic semiclassical frusta, together with the findings of [13], suggest that, if α allows for an intermediate spectral dimension $0 < D_{\mathrm{s}}^\alpha < 4$, the boundary term vanishes there. Consequently, D_{s}^α is given by

$$D_{\mathrm{s}}^\alpha = 2((9 - 12\alpha)V - n). \quad (4.18)$$

If the value of D_{s}^α lies outside the interval [0, 4], the boundary term counteracts to yield either zero or four. Because of the spatial homogeneity of frusta as well as the assumptions we introduced, the number of vertices V and the number configurations n are, respectively, given by $V = \mathcal{N}^4$ and $n = 2\mathcal{N}$. Plugging these expressions into Eq. (4.18) for $\mathcal{N} = 1$, the analytical estimate is compatible with the numerical findings of Sec. IV A as well as the previous results in [13].

Quantum amplitudes as well as semiclassical amplitudes for $\mathcal{N} > 1$ do not show a simple scaling behavior. However, what all these more general cases have in common is that they factorize into a scaling part and a nontrivial residual part. To capture this, we write

$$\mathcal{A}_v = r^{-\gamma_{\mathrm{cons}}} \mathcal{C}_v(r, \Omega), \quad (4.19)$$

where $\mathcal{C}_v(r, \Omega)$ can be understood as a *correction* term to the scaling part with constant γ_{cons}. Splitting the amplitudes into this form allows us to reexpress the spectral dimension as

$$D_{\mathrm{s}} = 2(\gamma_{\mathrm{cons}} V - n) - 2 \sum_v \frac{\int d\Omega dr r^{n-1} \frac{r}{\mathcal{C}_v} \frac{\partial \mathcal{C}_v}{\partial r} \prod_{v'} \mathcal{A}_{v'} \mathrm{Tr}(e^{\frac{\tau\Delta}{r}})}{\int d\Omega dr r^{n-1} \prod_{v'} \mathcal{A}_{v'} \mathrm{Tr}(e^{\frac{\tau\Delta}{r}})}$$
$$- 2 \frac{\partial I}{\langle P \rangle Z}. \quad (4.20)$$

For oscillating correction terms that attain many zeros, and therefore lead to divergences of the effective scaling, the integration domain of the above needs to be restricted accordingly. Aspects of well-definedness and convergence need to be addressed for each given $\mathcal{C}_v$ individually. Put into this form, Eq. (4.20) suggests that the pure scaling value of $D_{\mathrm{s}}^\alpha = 2((9 - 12\alpha)V - n)$ is corrected by a term arising from the effective scaling $-\frac{r}{\mathcal{C}_v} \frac{\partial \mathcal{C}_v}{\partial r}$ of the correction term $\mathcal{C}_v$ as well as the boundary term. Assuming that the boundary term is negligible in the regime of an intermediate spectral dimension, we compare the analytical estimate in Eq. (4.20) with the results of one-periodic quantum amplitudes, a cosmological constant for $\mathcal{N} = 1$ and finally the two-periodic case.

For $\alpha \gtrsim 0.24$, extrapolated quantum amplitudes exhibit an effective scaling larger than the semiclassical value, as Fig. 13 shows. This implies that

$$-\frac{r}{\mathcal{C}_v}\frac{\partial \mathcal{C}_v}{\partial r} > 0, \qquad (4.21)$$

and hence, that the spectral dimension is corrected to a larger value. This is exactly what we observe in Fig. 15.

In the presence of a cosmological constant Λ, the correction term in Eq. (4.4) is a shifted cosine with a quadratically scaling phase. Since the constant shift is smaller than 1, the correction terms hits many zeros, such that the effective scaling diverges at these points. Consequently, Eq. (4.20) is only valid on a restricted domain. Still, let $r_0^{(\Lambda)}$ denote the first zero of $\mathcal{C}_v$ depending on Λ. Then the effective scaling of $\mathcal{C}_v$ is larger than zero in the interval $[j_{\min}, r_0^{(\Lambda)}]$. This suggests that for growing τ, the first correction to the spectral dimension is to a larger value, which can be observed numerically in Sec. IV B. For the remaining integration range $r \in [r_0^{(\Lambda)}, j_{\max}]$, we conjecture that the rapidly changing scaling behavior is averaged out within the scales that are emphasized by $\mathrm{Tr}(e^{\frac{\tau\Delta}{r}})$. However, it is currently not in reach to substantiate this statement further.

Frusta amplitudes of periodicity $\mathcal{N} > 1$ exhibit a highly nontrivial correction term $\mathcal{C}_v(r, \Omega)$, as Eq. (4.10) indicates. Given that $\mathcal{C}_v$ hits many zeros, leading to divergences of its effective scaling, the integral in Eq. (4.20) has a highly restricted domain of validity which depends sensitively on the values of $(G, \gamma_{\mathrm{BI}}, \Lambda)$. Because of these obstacles for understanding the correction term, let us first consider a regime where $\mathcal{C}_v$ is approximately constant, obtained for large values of G, and comment on the more general case afterwards. In the absence of the correction and the boundary term, the intermediate spectral dimension is given by Eq. (4.18) for $V = 16$ and $n = 4$. The admissible values of α to observe an intermediate spectral dimension approximately lie in the interval [0.72, 0.73], as predicted by the analytical considerations.

Our numerical results of Sec. IV C are in partial accordance with this prediction. Qualitatively, we find an intermediate spectral dimension which is controlled solely by α, as Fig. 18 shows. Also, we find that the window of admissible α for such a regime is smaller compared to the one-periodic case. However, the qualitative predictions of the analytical arguments, notably Eq. (4.18), do not agree with the numerical results. In particular, the values of $\alpha_{\min}$ and $\alpha_{\max}$ as well as the values of D_s^α of the analytical derivation appear to be shifted with respect to the numerical ones. Recall that the whole analytical argument hinges on the assumption that the Laplacian exhibits a scaling behavior with a negligible angular dependence, given in Eq. (4.11). While this might be justified for $\mathcal{N} = 1$, the angular dependence of Δ for $\mathcal{N} > 2$ is more intricate. Therefore, we suspect this assumption to be the main source of the discrepancy between the analytical predictions and the numerical results. As a result, changes of the intermediate dimension which are not captured by Eq. (4.18) are

conceivable. Still, we recall that the window of intermediate scales $j_{\min} < \tau < j_{\max}$ for the results of Sec. IV C is small, necessitating further analysis of the qualitative inconsistency between analytical and numerical results.

When correction terms cannot be neglected, i.e. when the value of the action S_R is of order G, the spectral dimension is sensitive to the values of G and Λ, as the numerical results of Sec. IV C show. In the intermediate regime $j_{\min} < \tau < j_{\max}$ one observes corrections to D_s^α for some (G, Λ) to smaller as well as to larger values. Moreover, the window $[\alpha_{\min}, \alpha_{\max}]$ is shifted depending on G and Λ. This suggests that for higher periodicities, the correction term is predominant, introducing an intricate dependence of the intermediate dimension on the parameter values (α, G, Λ).

2. An integrable model with oscillations

Faced with the obstacle of computing the corrections of oscillating terms explicitly, we consider in the following a simplified integrable system. The results we derive support the intuition we have attained in the preceding part of this section.

The simplified model is an equilateral lattice. We find closed expressions for the heat trace in one dimension, though the results should extend to hypercubic lattices of any dimension since the lattice heat trace factorizes [69]. On the one-dimensional lattice, it is possible to integrate the heat trace

$$P_{1\mathrm{D}}(x) := \int_0^\pi \mathrm{d}p\, e^{-x(1-\cos p)} = \pi e^{-x} I_0(x) \qquad (4.22)$$

where I_0 is the modified Bessel function. For this, integration with a purely scaling measure (constant $\gamma = \gamma_{\mathrm{cons}}$) gives

$$\langle P(\tau)\rangle_\gamma := \int_{j_{\min}}^{j_{\max}} \mathrm{d}r\, r^{-\gamma} P_{1\mathrm{D}}(\tau/r)$$

$$= \frac{\pi}{1-\gamma} r^{1-\gamma}\,{}_2F_2\left(\begin{matrix}\frac{1}{2}, & \gamma-1\\ 1, & \gamma\end{matrix};-2\tau/r\right)\Bigg|_{j_{\min}}^{j_{\max}}, \qquad (4.23)$$

where ${}_pF_q\binom{a_1,\ldots,a_p}{b_1,\ldots,b_q};z)$ is the generalized hypergeometric function.[21] In the regime $j_{\min} \ll \tau \ll j_{\max}$, this example gives the expected spectral dimension $D_s = 2(\gamma - 1)$, presented in Fig. 22. In particular, one finds this value as the exact constant result for the integral with $j_{\min} = 0$ and $j_{\max} = \infty$.

This example can still be integrated with an oscillating measure over the positive reals,

---

[21]For an explicit definition of the generalized hypergeometric function ${}_pF_q$, see for instance [82].
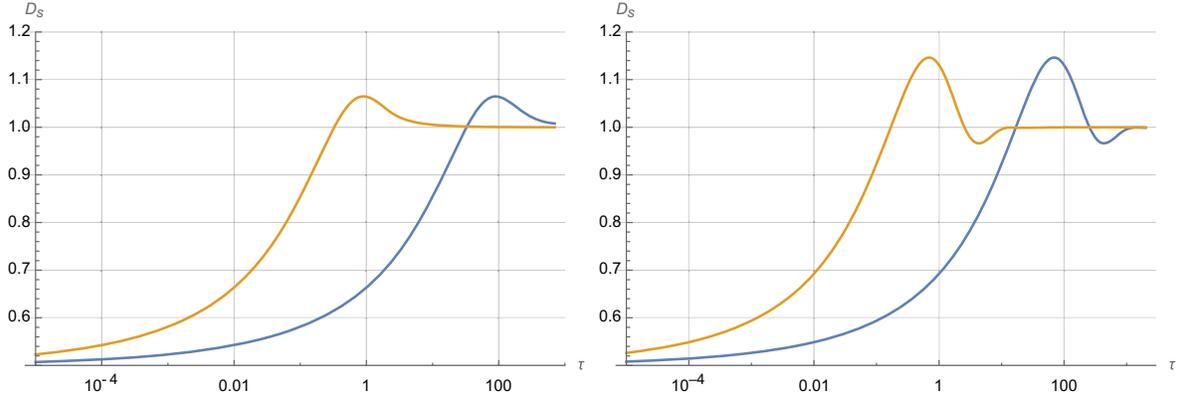
FIG. 22. Left: Spectral dimension of superposed one-dimensional lattice geometries with purely scaling measure, $\gamma = \frac{5}{4}$, integrated from $j_{\min} = 0$ to $j_{\max} = 1$ (yellow) and $j_{\max} = 100$ (blue). Right: The same for an oscillating measure integrated from $j_{\min} = 0$ to $j_{\max} = \infty$, with $\gamma = \frac{5}{4}$ and $\omega = 1$ (yellow) and $\omega = 1/100$ (blue).

$$\langle P(\tau) \rangle_{\gamma,\omega} := \int_0^\infty r^{-\gamma} \cos(\omega r) \mathrm{d}r P_{1D}(\tau/r). \tag{4.24}$$

Interestingly, the result turns out to be a function solely in the combined variable $\omega\tau$ up to a factor $\omega^{\gamma-1}$,

$$\langle P(\tau) \rangle_{\gamma,\omega} = \sqrt{\pi} \frac{\Gamma(\frac{3}{2} - \gamma)\Gamma(\gamma - 1)}{\Gamma(2 - \gamma)} (2\tau)^{1-\gamma} {}_2F_5\left(\begin{matrix} \frac{3-2\gamma}{4}, \frac{5-2\gamma}{4} \\ \frac{1}{2}, \frac{2-\gamma}{2}, \frac{2-\gamma}{2}, \frac{3-\gamma}{2}, \frac{3-\gamma}{2} \end{matrix}; -(\omega\tau)^2/4 \right)$$
$$- \omega^{\gamma-1} \pi \Gamma(-\gamma) \left[\cos(\pi\gamma/2) \omega\tau {}_2F_5\left(\begin{matrix} \frac{3}{4}, \frac{5}{4} \\ 1, \frac{3}{2}, \frac{3}{2}, \frac{1+\gamma}{2}, \frac{2+\gamma}{2} \end{matrix}; -(\omega\tau)^2/4 \right) \right.$$
$$\left. + \gamma \sin(\pi\gamma/2) {}_2F_5\left(\begin{matrix} \frac{1}{4}, \frac{3}{4} \\ \frac{1}{2}, \frac{1}{2}, 1, \frac{1+\gamma}{2}, \frac{\gamma}{2} \end{matrix}; -(\omega\tau)^2/4 \right) \right].$$

As a consequence, the spectral dimension is also a function in $\omega\tau$. Surprisingly, even though there are no boundary terms, this spectral dimension shows a flow from $2(\gamma - 1)$ to $D_s = 1$ with an intermediate maximum at $\tau \approx 1/\omega$ directly followed by a local minimum already close to $D_s = 1$; see Fig. 22. For a finite upper integration boundary $j_{\max} > \omega\tau$ we would therefore expect no significant difference.

The spin foam measure in Eq. (4.4) that we want to model has a correction which is a linear combination of a constant term and an oscillating one. Thus, we have to consider the spectral dimension of the combination $a\langle P(\tau) \rangle_\gamma + \langle P(\tau) \rangle_{\gamma,\omega}$, that is, the quantity

$$D_s(\tau) = -2\tau \frac{a\partial_\tau \langle P(\tau) \rangle_\gamma + \partial_\tau \langle P(\tau) \rangle_{\gamma,\omega}}{a\langle P(\tau) \rangle_\gamma + \langle P(\tau) \rangle_{\gamma,\omega}}. \tag{4.25}$$

From earlier work [69] we know that a linear combination of two heat trace expectation values $\langle P(\tau) \rangle_\gamma$ and $\langle P(\tau) \rangle_{\gamma'}$ with different scalings $\gamma > \gamma'$ leads to a spectral dimension of value $2(\gamma - 1)$ followed by a value $2(\gamma' - 1)$ at larger scale τ. Something similar happens in the linear combination here when $j_{\max} \gg 1/\omega$: As Fig. 23 shows, we see
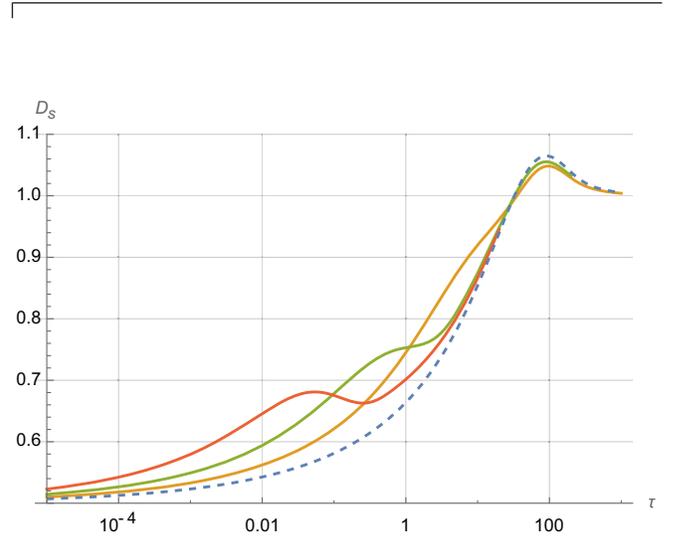
FIG. 23. Spectral dimension of superposed one-dimensional lattice geometries with a combined measure, Eq. (4.25), with $j_{\min} = 0$, $j_{\max} = 100$ (in the scaling part), a relative factor $a = 1.5$, and oscillations $\omega = 10, 1, 1/10$ (with resulting peaks at $\tau \sim 1/\omega$ from left to right); the purely scaling case is given for comparison as dashed curve.

the oscillation peak of the $\langle P(\tau)\rangle_{\gamma,\omega}$ part at $\omega\tau \approx 1$ but after that the $\langle P(\tau)\rangle_{\gamma}$ part dominates. Together, this yields a spectral dimension which looks like the purely scaling part with an extra local maximum superposed at scale $\tau \approx 1/\omega$. This is exactly the qualitative behavior found in Fig. 16. In this way, the simplified example gives an explanation of the mechanism underlying the effect of a cosmological constant on the spectral dimension of spin foams.

V. DISCUSSION

A. Renormalization and the spectral dimension

From the perspective of classical general relativity, return probability and spectral dimension are reasonable observables. The return probability is coordinate independent since it is a trace of the heat kernel over the entire space-time. Equivalently, it is given by the exponentiated integral of the spectrum of the Laplace operator. Therefore it should be a suitable observable in the context of quantum gravity.

Diffeomorphism invariance is typically broken in spin foam models, yet we expect its restoration to be tied to (a notion of) discretization independence [43–45,52,53,83–86]. This is vital if we interpret the spin foam two-complex as a fiducial object, providing a regularization of the theory. Then, predictions of the theory must be consistent for different regulator choices, i.e., the regulator can be removed and the observables remain well defined in a suitable refinement limit. In principle this logic should apply to the spectral dimension as well, yet it is more subtle.

To point out the particularities of renormalization in a background independent setting, it is helpful to first consider the spectral dimension on two different discretizations of the same manifold, where one is the refinement of the other. For diffusion times much larger than the typical length scale of the triangulation, their spectral dimension will agree with the continuum result. By definition, for the coarser triangulation this scale is larger; therefore, its spectral dimension will deviate from the continuum result for larger diffusion compared to the finer triangulation. This is perfectly expected as the coarser triangulation is ignorant to dynamics below its discretization scale. In the context of spin foams however, this question is more intricate.

In a spin foam setting, consider two two-complexes, where the coarser one arises from coarse graining the fine one. Let us additionally assume that we can compute the coarse graining flow of spin foam amplitudes, such that we can assign a theory to the fine two-complex and its coarse grained version to the coarse one. Crucially, in a background independent theory, the discretization scale is not a parameter but part of the variables we are summing over. Thus, instead of the scale, the difference between coarse and fine theory is that the fine theory features more variables and can thus capture more configurations than the coarse one. Some of these fine configurations will correspond to representations of coarse configurations on the finer discretization, between which one could relate with embedding maps, yet some configurations cannot be captured in the coarse case. Therefore, one would expect differences to occur when the spectral dimension probes these fine configurations, assuming one is using the same definition of Laplace operator. This might be avoided by also coarse graining the Laplace operator such that the coarse version effectively reflects how the scalar field probes the fine version configurations leading to a modified spectrum of the renormalized operator.[22] However, this procedure is ambitious and goes beyond the scope of this article.

Another method to employ a refinement limit is to study the same observable on finer and finer two-complexes, with the same theory assigned to each complex. This is closer to the setup of this article, but strictly speaking not a renormalization procedure. The idea is to send the number of building blocks to infinity with the goal to identify whether the observable converges under refinement; and further whether there are indications for a phase transition, if it is indeed an order parameter for this transition. In this way one might determine the set of parameters for which the original theory approximates a potential fixed point. Close to such a fixed point, discretization independence would be approximately satisfied.[23]

Beyond the technical challenges, one must first define how to systematically refine the two-complex in order to define such a limit (if it indeed exists). In our setup of $\mathcal{N}$-periodic spin foams on hypercubic lattices, this is straightforwardly the limit $\mathcal{N} \to \infty$, which simultaneously removes the assumption of periodicity. To distinguish this limit from the refinement limit as determined by a renormalization procedure,[24] we call the limit $\mathcal{N} \to \infty$ together with $j_{\max} \to \infty$ the thermodynamic limit. We discuss the implications of our analytical results for the thermodynamic limit in the next section.

B. The thermodynamic limit

Several assumptions underlie the numerical results of Sec. IV, the strongest of which is clearly that of $\mathcal{N}$ periodicity of the geometric configurations. Furthermore,

---

[22]The interpretation is that the coarse theory arises as an effective dynamics from the fine one after integrating out fine degrees of freedom. This would apply to the scalar field even though it is unphysical.

[23]Conceptually, the ideas outlined here can be straightforwardly applied for two-complexes without a boundary. For two-complexes with a boundary, one still needs to relate boundary states in different Hilbert spaces to describe the same transition.

[24]It is not straightforward to implement $\mathcal{N}$ periodicity in a coarse graining procedure: imagine coarse graining an $\mathcal{N}$-periodic spin foam such that the number of degrees of freedom are halved. Unfortunately, without additional restrictions the resulting spin foam will not be an $\mathcal{N}/2$-periodic spin foam.

we truncated the number of dressed vertex amplitudes to $\mathcal{N}$ and introduced an upper cutoff $j_{\max}$ for a feasible numerical implementation. Both the cutoff and the periodicity need to be removed for physically viable results in the limits $j_{\max} \to \infty$ and $\mathcal{N} \to \infty$, respectively. In the following, we discuss these limits and the resulting interpretation of the spectral dimension.

As shown, the cutoffs $j_{\min}$ and $j_{\max}$ mark the boundaries for the scale τ between which an intermediate spectral dimension is possible; outside these values it flows to the value zero and four, respectively. In the limit $j_{\max} \to \infty$, we therefore expect an indefinite continuation of the intermediate regime to large scales. Because of the restrictive value of $j_{\max} = 201$ in Sec. IV C and the intricate form of $\mathcal{C}_v$ for $\mathcal{N} > 1$ in Sec. IV D, inferring the explicit form of this continued intermediate regime for $\mathcal{N} \geq 2$ remains an open challenge. Further, the simplified integrable model of Sec. IV D 2 has shown that oscillations can result in a flow to the topological dimension around the scale given by the frequency of the oscillations independent of an upper cutoff. Whether this generalizes to the intricate oscillatory dependence of spin foams is an intriguing direction for future research.

The plateau of the spectral dimension for purely scaling amplitudes, given in Eq. (4.18), depends on the number of configuration variables n as well as the number of vertices V. Within the approximations we have imposed, n and V are related to the periodicity $\mathcal{N}$ via $n = 2\mathcal{N}$ and $V = \mathcal{N}^4$, respectively. Then, the interval $[\alpha_{\min}, \alpha_{\max}]$, for which an intermediate dimension $0 < D_s^\alpha < 4$ exists can be reexpressed in terms of $\mathcal{N}$

$$\alpha_{\min} = \frac{1}{12}\left(9 - \frac{2\mathcal{N}+2}{\mathcal{N}^4}\right), \quad \alpha_{\max} = \frac{1}{12}\left(9 - \frac{2\mathcal{N}}{\mathcal{N}^4}\right). \quad (5.1)$$

Clearly, in the limit $\mathcal{N} \to \infty$, the interval shrinks to a single point α_*, corresponding to the value at which the amplitudes are scale invariant. This is due to the fact that we are considering higher and higher powers of the amplitudes. Following [13], in the context of cuboids, this point marks a phase transition since the spectral dimension changes discontinuously from 0 to 4 at α_*. Since the degrees of freedom as well as the combinatorial length $L = \mathcal{N}$ are taken to infinity while keeping their ratio fixed, $\mathcal{N} \to \infty$ corresponds to a thermodynamic limit. Numerical results for one-periodic frusta, presented in Sec. IV A, are in alignment with the analytical formula in Eq. (4.18). Also, the interval $[\alpha_{\min}, \alpha_{\max}]$ of admissible α values to observe such an intermediate regime are supported by our results.

Generalizing to two-periodic or higher configurations, the parameter space of the theory extends as the amplitudes now depend on $(\alpha, G, \gamma_{\mathrm{BI}}, \Lambda)$. Qualitatively, for fixed $(G, \gamma_{\mathrm{BI}}, \Lambda)$, we still observe that α controls the value of

the intermediate dimension and that the interval between $\alpha_{\min}$ and $\alpha_{\max}$ is smaller in comparison to the one-periodic case. This suggests that a similar argument as in [13] applies: In the limit $\mathcal{N} \to \infty$, the spectral dimension exhibits a nontrivial flow only when α is tuned to some fixed value α_*. Notice that, in comparison to cuboids, frusta amplitudes are strictly speaking *never* scale invariant. Consequently, α_* is in general not given by $\alpha_* = \frac{3}{4}$. Crucially, we observe that $(G, \gamma_{\mathrm{BI}}, \Lambda)$ impact the spectral dimension only in the intermediate regime, which is controlled by α. Conversely, outside the relevant α interval, we did not observe these parameters inducing a change in the spectral dimension.

If we vary $(G, \gamma_{\mathrm{BI}}, \Lambda)$, the value α_* might change, in principle, and become a function of these parameters. Geometrically, this would imply in general a nontrivial surface Σ_* of codimension one in four-dimensional parameter space $(\alpha, G, \gamma_{\mathrm{BI}}, \Lambda)$ which marks the phase transition in the limit $\mathcal{N} \to \infty$. As demonstrated in Sec. IV C, the values of $\alpha_{\min}$ and $\alpha_{\max}$ are indeed dependent on G and Λ.[25] In the limit $\mathcal{N} \to \infty$, the interval of α's will shrink to a point, the value of which depends on G, γ_{BI}, and Λ. Consequently, $\alpha_*(G, \gamma_{\mathrm{BI}}, \Lambda)$ defines a nontrivial embedded surface Σ_* which, tentatively speaking, marks the critical surface of a phase transition.

Taking the perspective that γ_{BI} and α are fixed and nonflowing parameters,[26] the intersection of the α and γ_{BI} hypersurfaces together with Σ_* yield the lines of (G, Λ), which we interpret as critical lines. A graphical intuition for that is presented in Fig. 24 with the γ_{BI}-direction suppressed. This intersection might also be empty though, depending on the values of α and γ_{BI}.

In light of the previous discussion on renormalization, we emphasize that the large-$\mathcal{N}$ limit is not to be understood as a renormalization flow but rather as a removal of the $\mathcal{N}$-periodicity assumption. Defining a spin foam renormalization flow requires a refinement of the combinatorial structure as well as a relation between coarse and fine geometric variables. In contrast, the large-$\mathcal{N}$ limit simply considers the addition of building blocks and does not affect the variables or the states. Consequently, the RG-fixed points are in general not related to the "critical values" $(\alpha_*, G_*, \gamma_{\mathrm{BI}*}, \Lambda_*)$ of the limit $\mathcal{N} \to \infty$, but might provide indications for such a fixed point.

---

[25] We fixed γ_{BI} to render the simulations feasible. However, if not fixed by other arguments such as from black hole entropy matching [87], we expect that γ_{BI} plays a similar role as G and Λ, influencing the value of α_*. We therefore assume in the following that α_* depends also on γ_{BI}.

[26] Matching the black hole entropy from LQG to the Bekenstein-Hawking formula requires γ_{BI} to take a specific value [87]. We remind the reader that α parametrizes an ambiguity in the face amplitudes. Choosing a specific model with a given face amplitude therefore corresponds to a fixed nonflowing α.
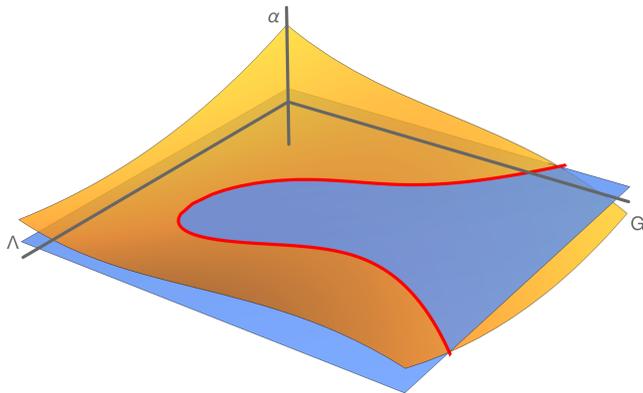
FIG. 24.   Sketch of a critical surface Σ_* in the parameter space of theory with the γ_{BI} direction suppressed. Given that α is fixed (blue plane), the intersection with Σ_*, indicated by the red curve, marks the critical values of G and Λ.

C. Information about G, Λ and γ_{BI} from the spectral dimension

As demonstrated in Sec. IV B and Sec. IV C, Newton's constant G and the cosmological constant Λ have an immediate effect on the flow of the spectral dimension. It is furthermore to be expected that γ_{BI} plays a similar role for frusta of $\mathcal{N} > 2$. In principle, this could open the possibility to extract the values of G, γ_{BI}, and Λ in a given regime from determining the effective, spectral dimension. In this section we discuss this possibility and its limitations.

Consider the one-periodic case discussed in Sec. IV B first, where the Regge curvature vanishes and only the ratio Λ/G becomes relevant. Given that an intermediate regime exists, the spectral dimension will locally flow to a larger value in the vicinity of the scale at which the amplitude completes the first oscillation. This scale is directly related to the value of Λ/G. In principle, a given one-periodic spectral dimension flow therefore provides insight to the value of Λ/G.

This picture changes drastically when going to higher periodicities where $S_R \neq 0$. In these cases the flow of the spectral dimension is highly sensitive to the three parameters $(G, \gamma_{BI}, \Lambda)$, where the effects do not seem to be localized around a certain scale. Again, a given measurement of the spectral dimension could, in principle, be used to attain partial knowledge on the values of these parameters. Various caveats and limitations follow these suggestions, the most important ones of which we discuss in the following.

First, for computing the two-periodic spectral dimension we have employed semiclassical amplitudes. Therefore, quantum effects have been neglected on small scales $\tau \sim j_{min}$. Such effects have presented themselves in two ways. As discussed in Sec. IV A, quantum amplitudes show a nonconstant modified scaling behavior. Following [51], oscillating quantum amplitudes also show a phase shift with respect to the semiclassical ones on low scales.

Clearly, both of these quantum effects need to be taken into account when considering the spectral dimension as an observable quantity.

Second, the results of Sec. IV C suggest that the map between the parameters $(G, \gamma_{BI}, \Lambda)$ and the corresponding spectral dimension is only surjective, such that one cannot extract a unique triple $(G, \gamma_{BI}, \Lambda)$ from a measured flow of D_s. Moreover, for $\mathcal{N} > 1$, the amplitudes exhibit an intricate oscillatory behavior which leads to a spectral dimension that is highly sensitive to the values of $(G, \gamma_{BI}, \Lambda)$. Indeed, we expect that it is necessary to measure several observables to determine these parameters accurately. Nevertheless, knowing D_s for all scales contains a lot of, albeit coarse grained, information of quantum space-time that should allow us to constraint the range of admissible parameters, e.g., to distinguish whether G is large or small.

Third, the triple $(G, \gamma_{BI}, \Lambda)$ entering the semiclassical amplitudes in Eq. (2.13) is considered as the *bare* parameters.[27] Thus, under a renormalization flow and under the assumption that we project back onto the original theory space, e.g., as in [31], it is, in general, to be expected that $(G, \gamma_{BI}, \Lambda)$ flow as well. As stressed above, for physical viability, the spectral dimension must be considered at a fixed point of the renormalization group flow to ensure discretization independence of the result. The values of $(G, \gamma_{BI}, \Lambda)$ at this fixed point are then the quantities that can be, in principle, observed.

An observable effect of the parameters on the spectral dimension requires the existence of an intermediate regime. As discussed in Sec. V B, in the thermodynamic limit $j_{max} \to \infty$ and $\mathcal{N} \to \infty$, the values of $(\alpha, G, \gamma_{BI}, \Lambda)$ for which such a regime exists shrink to a point. At this transition point, the spectral dimension is expected to show a nontrivial behavior. However, with the assumptions of finite upper cutoff j_{max} and periodicity $\mathcal{N}$, necessary for the computations in Sec. IV, determining the spectral dimension at the transition point is currently out of reach.

As a last caveat, we remind the reader that the model we consider here presupposes a Euclidean space-time signature. The kinematics of physical scalar fields is governed by the d'Alembert operator and not the four-dimensional Laplace operator. Hence, deviations between predictions based on Euclidean models and results from measurements are in general to be expected. In addition to Lorentzian effects, we recall that the Laplace operator was defined via its action on scalar test fields. Physical fields used for actual measurements couple nontrivially to the geometry of space-time and lead to backreactions on the gravitational field; see, e.g., [54]. As a result, the spectrum of the Laplace operator and therefore the return probability as well as the

---

[27]This is discussed in more detail in the previous two sections. For discussion on the flow of γ_{BI}, we refer the interested reader to [88].

scaling behavior of spin foam and matter amplitudes are modified.

VI. CONCLUSIONS

In this work, we have studied the effects of quantum amplitudes and oscillations on the spectral dimension within the EPRL-FK model, restricted to $\mathcal{N}$-periodic frusta geometries. This marks a significant expansion of previous work [13] on flat, nonoscillatory and purely semiclassical cuboid geometries [52]. To bypass the steep numerical costs for computing quantum frusta amplitudes already at small spins [51], we have presented a method to extrapolate quantum amplitudes for $\mathcal{N} = 1$ to large spins in Sec. III, serving as an improved approximation compared to semiclassical amplitude, in particular, at low spins. This marks the first result of our work.

Computing the spectral dimension with respect to extrapolated amplitudes, we find additive corrections at low scales compared to the semiclassical results. Supported by analytical computations, these quantum corrections can be traced back to a modified effective scaling behavior of the extrapolated amplitudes, constituting our second result.

As a third result we have found that curvature induced by a cosmological constant Λ yields additive corrections of the one-periodic spectral dimension at scales $\tau \sim 1/\sqrt{\Lambda}$. We have shown that such effects of Λ can also be understood qualitatively by considering the effective scaling of the amplitudes. Furthermore, we have given an explanation of the mechanism underlying these results in terms of a simplified integrable model with such oscillating measure.

Finally, we found that two-periodic amplitudes with an intricate oscillatory behavior lead to a flow of the spectral dimension which depends on the full set of parameters $(\alpha, G, \gamma_{\mathrm{BI}}, \Lambda)$. Summarizing, our numerical and analytical results show that curvature is an essential factor for the spectral dimension that requires further study.

In an overarching perspective, the results of the present work are an intermediate step towards understanding the spectral dimension of more general quantum geometries. Spin foam frusta with their inherent high degree of symmetry present a strong restriction of the quantum geometry compared to the general case. Retaining hypercubic combinatorics, a feasible scenario would be to construct a more general restricted model, which however quickly becomes cumbersome and the numerical challenges in the quantum regime remain. Furthermore, there is evidence that the EPRL-FK model for higher valent vertices differs from the one defined on triangulations in the implementation of simplicity constraints [89,90], and geometric critical points with torsion and nonmetricity exist [52,91]. Therefore, if all restrictions on the geometry are lifted, it is advantageous to directly work on triangulations, where the semiclassical amplitudes are well studied [32,33,92–96] and more numerical methods are available and in development [35–37,41,47].

In the following, we briefly discuss the challenges one faces when defining the spectral dimension on unrestricted spin foams defined on a triangulation.

  (i) *$\mathcal{N}$-periodicity on a triangulation:* The introduction of $\mathcal{N}$-periodicity [13] is highly beneficial for reducing the computational effort. In particular, formulating the spectrum of the Laplace operator on momentum space is far more efficient than directly diagonalizing the Laplace operator and can be straightforwardly generalized to larger two-complexes. The notion of $\mathcal{N}$ periodicity is tied to combinatorial "directions," which are naturally defined on a hypercubic lattice. On four-dimensional triangulations these intuitions are not applicable and $\mathcal{N}$ periodicity is not straightforwardly defined.

 (ii) *Vector geometries in the semiclassical limit:* The semiclassical amplitudes for a four-simplex exhibit different types of critical points, depending on the boundary data [32]. While Regge geometries present one class of solutions, so-called vector geometries [32] contribute with the same degree of polynomial decay. Since such configurations do not correspond to geometric four-simplices, their four-volume is not defined, and it is not obvious how to generalize the definition of a Laplace operator.

(iii) *Nonmatching simplices/complex critical points:* The restriction to cuboid or frusta geometries is special, as each 4D building block is evaluated on a critical point and glued along matching 3D polyhedra. In recent years, there has been growing evidence that configurations beyond real critical points must be taken into account for large, but finite spins. In effective spin foams [37,40] and the hybrid algorithm representation [36] these are parametrized as geometric but nonmatching simplices, i.e., the shared 3D building blocks have different shapes as seen from their 4D building blocks. Alternatively, such configurations are called complex critical points [41,50]: such configurations can be interpreted as exhibiting nonvanishing torsion and play an important role in understanding and circumventing the flatness problem [37,50,97–100]. Following our definition, the Laplace operator for such a nonmatching configuration might not be symmetric any more.

 (iv) *Pregeometric configurations:* Beyond a modified scaling behavior, the deep quantum regime of spin foams additionally features pregeometric configurations which are not peaked (as coherent states) on the shape of semiclassical polyhedra. It is an intriguing question how a scalar test field can probe such a quantum geometry.

  (v) *Numerical challenges in and beyond the quantum regime:* Although the computation of quantum amplitudes is more feasible in the general simplicial

case, the mere number of ten spin configurations per vertex presents serious numerical challenges.

(vi) *Lorentzian signature:* The studies of the spectral dimension presented here essentially examine a diffusion process on Euclidean quantum space-time. It will be interesting to see whether these concepts can be generalized to Lorentzian test fields probing a Lorentzian quantum space-time; see, e.g., [101] for an implementation in causal set theory. For the gravitational side, choosing the Lorentzian EPRL-FK model might be beneficial compared to the Euclidean one: semiclassical Lorentzian four-simplices feature oscillations proportional to γ_{BI}.

We expect that several of the features mentioned above will have an impact on the spectral dimension, which we currently cannot estimate. In particular, it will be interesting to see whether the effective scaling of the amplitudes can still explain the behavior of the spectral dimension if pregeometric configurations are considered. Therefore, it is imperative to lift the restrictions of the frusta model and work towards exploring the spectral dimension on unrestricted spin foam quantum geometries.

A possibility to define $\mathcal{N}$ periodicity in a simplicial context could be to triangulate $\mathcal{N}$-periodic cubical lattices. There exist several inequivalent options to realize that, two examples of which are given in [102,103], respectively. Geometrically, these configurations correspond to different triangulations of the torus. Explicitly setting up $\mathcal{N}$-periodic triangulations and computing the spectral dimension thereof is left for future work.

Within the context of spin foam frusta, a conceivable method to compute the spectral dimension for higher periodicities and larger cutoffs j_{max} is to restrict to configurations with small dihedral angles, e.g., via a Gaussian. Previous work [13] supports the conjecture that this restriction still captures the relevant geometric information. If valid, this reduction of configurations would greatly simplify the numerical effort required to compute D_s, enabling exploration of regimes currently out of reach. Also for less restricted geometries on a triangulation, a linearization around flat configurations could be advantageous as this simultaneously simplifies the form of the amplitudes and the Laplace operator.

Going beyond small periodicities is numerically challenging regardless of the specific model at hand. This is even more true for triangulations without geometric restrictions, where we must consider vastly more variables compared to the symmetry restricted frusta cases. To reliably compute expectation values of observables, it is therefore imperative to use a numerical method that does not exponentially scale with the number of variables of the system. In many areas of physics, Monte Carlo methods serve this role, yet cannot be readily applied in spin foams. Because of the oscillatory nature of spin foam amplitudes, the spin foam partition function might not be naively usable as a probability distribution to sample results with. A way around this might be to define Markov Chain Monte Carlo on Lefschetz thimbles of the spin foam partition function [39], where the integration contour is changed such that the imaginary part of the system is constant and thus nonoscillatory. Alternatively, a potential strategy might be to propose a new probability distribution to sample configurations with. Recently, random sampling of bulk quantum numbers was applied to approximate spin foam amplitudes with many bulk faces in [49].

To conclude, the spectral dimension remains an intriguing observable in spin foam models that is far from understood. Our results show that its value at small scales depends on all the parameters $\alpha, G, \gamma_{BI}, \Lambda$, though the specific relations are sensitive to the specific restricted model. Many effects such as pregeometric configurations might alter its behavior. Hence, our work shows how the spectral dimension of spin foam geometry can provide us with a deeper, coarse grained understanding of quantum space-time while at the same time allowing us to connect to other approaches of quantum gravity as well as continuum physics.

[1] C. Rovelli, Zakopane lectures on loop gravity, in Proc. Sci. QGQGS2011 (**2011**) 003.

[2] A. Ashtekar and J. Lewandowski, Background independent quantum gravity: A status report, Classical Quantum Gravity **21**, R53 (2004).

[3] A. Pérez, The spin-foam approach to quantum gravity, Living Rev. Relativity **16**, 3 (2013).

[4] L. Freidel, Group field theory: An overview, Int. J. Theor. Phys. **44**, 1769 (2005).

[5] D. Oriti, The microscopic dynamics of quantum space as a group field theory, in *Foundations of Space and Time* (Cambridge University Press, Cambridge, UK, 2012).

[6] S. Carrozza, Tensorial methods and renormalization in group field theories, Ph.D. thesis, Orsay, LPT, 2013.

[7] R. Loll, Quantum gravity from causal dynamical triangulations: A review, Classical Quantum Gravity **37**, 013002 (2020).

[8] J. Ambjorn, A. Görlich, J. Jurkiewicz, and R. Loll, Nonperturbative quantum gravity, Phys. Rep. **519**, 127 (2012).

[9] S. Surya, The causal set approach to quantum gravity, Living Rev. Relativity **22**, 5 (2019).

[10] F. Dowker, Introduction to causal sets and their phenomenology, Gen. Relativ. Gravit. **45**, 1651 (2013).

[11] P. Di Francesco, P. Ginsparg, and J. Zinn-Justin, 2D gravity and random matrices, Phys. Rep. **254**, 1 (1995).

[12] R. Gurau and J. P. Ryan, Melons are branched polymers, Ann. Henri Poincaré **15**, 2085 (2014).

[13] S. Steinhaus and J. Thürigen, Emergence of spacetime in a restricted Spin-foam model, Phys. Rev. D **98**, 026013 (2018).

[14] S. J. Carlip, Dimension and dimensional reduction in quantum gravity, Classical Quantum Gravity **34**, 193001 (2017).

[15] L. Crane and L. Smolin, Space-time foam as the universal regulator, Gen. Relativ. Gravit. **17**, 1209 (1985).

[16] L. Crane and L. Smolin, Renormalization of general relativity on a background of spacetime foam, Nucl. Phys. **267**, 714 (1986).

[17] J. Ambjorn, J. Jurkiewicz, and R. Loll, Reconstructing the Universe, Phys. Rev. D **72**, 064014 (2005).

[18] D. N. Coumbe and J. Jurkiewicz, Evidence for asymptotic safety from dimensional reduction in causal dynamical triangulations, J. High Energy Phys. 03 (2015) 151.

[19] O. Lauscher and M. Reuter, Fractal spacetime structure in asymptotically safe gravity, J. High Energy Phys. 10 (2005) 050.

[20] P. Horava, Spectral Dimension of the Universe in Quantum Gravity at a Lifshitz Point, Phys. Rev. Lett. **102**, 161301 (2009).

[21] D. Benedetti, Fractal Properties of Quantum Spacetime, Phys. Rev. Lett. **102**, 111303 (2009).

[22] E. Alesci and M. Arzano, Anomalous dimension in three-dimensional semiclassical gravity, Phys. Lett. B **707**, 272 (2012).

[23] M. Arzano and T. Trzesniewski, Diffusion on κ-Minkowski space, Phys. Rev. D **89**, 124024 (2014).

[24] M. Eckstein and T. Trześniewski, Spectral dimensions and dimension spectra of quantum spacetimes, Phys. Rev. D **102** (2020).

[25] M. Reitz, D. Németh, D. Rajbhandari, A. Görlich, and J. Gizbert-Studnicki, Generalised spectral dimensions in non-perturbative quantum gravity, Classical Quantum Gravity **40**, 125003 (2023).

[26] G. Calcagni, D. Oriti, and J. Thürigen, Spectral dimension of quantum geometries, Classical Quantum Gravity **31**, 135014 (2014).

[27] G. Calcagni, D. Oriti, and J. Thürigen, Dimensional flow in discrete quantum geometries, Phys. Rev. D **91**, 084047 (2015).

[28] A. Eichhorn, S. Mizera, and S. Surya, Echoes of asymptotic silence in causal set quantum gravity, Classical Quantum Gravity **34**, 16LT01 (2017).

[29] G. Calcagni, S. Kuroyanagi, S. Marsat, M. Sakellariadou, N. Tamanini, and G. Tasinato, Quantum gravity and gravitational-wave astronomy, J. Cosmol. Astropart. Phys. 10 (2019) 012.

[30] B. Bahr, S. Klöser, and G. Rabuffo, Towards a cosmological subsector of spin foam quantum gravity, Phys. Rev. D **96**, 086009 (2017).

[31] B. Bahr, G. Rabuffo, and S. Steinhaus, Renormalization of symmetry restricted spin foam models with curvature in the asymptotic regime, Phys. Rev. D **98**, 106026 (2018).

[32] J. W. Barrett, R. J. Dowdall, W. J. Fairbairn, H. Gomes, and F. Hellmann, Asymptotic analysis of the Engle-Pereira-Rovelli-Livine four-simplex amplitude, J. Math. Phys. (N.Y.) **50**, 112504 (2009).

[33] J. W. Barrett, R. J. Dowdall, W. J. Fairbairn, F. Hellmann, and R. Pereira, Lorentzian spin foam amplitudes: Graphical calculus and asymptotics, Classical Quantum Gravity **27**, 165009 (2010).

[34] P. Don, M. Fanizza, G. Sarno, and S. Speziale, SU(2) graph invariants, Regge actions and polytopes, Classical Quantum Gravity **35**, 045011 (2018).

[35] P. Donà, M. Fanizza, G. Sarno, and S. Speziale, Numerical study of the Lorentzian Engle-Pereira-Rovelli-Livine spin foam amplitude, Phys. Rev. D **100**, 106003 (2019).

[36] S. K. Asante, J. D. Simão, and S. Steinhaus, Spin-foams as semiclassical vertices: Gluing constraints and a hybrid algorithm, Phys. Rev. D **107**, 046002 (2023).

[37] S. K. Asante, B. Dittrich, and H. M. Haggard, Effective Spin Foam Models for Four-Dimensional Quantum Gravity, Phys. Rev. Lett. **125**, 231301 (2020).

[38] S. K. Asante, B. Dittrich, and H. M. Haggard, Discrete gravity dynamics from effective spin foams, Classical Quantum Gravity **38**, 145023 (2021).

[39] M. Han, Z. Huang, H. Liu, D. Qu, and Y. Wan, Spinfoam on a Lefschetz thimble: Markov chain Monte Carlo computation of a Lorentzian spinfoam propagator, Phys. Rev. D **103**, 084026 (2021).

[40] S. K. Asante, B. Dittrich, and J. Padua-Arguelles, Effective spin foam models for Lorentzian quantum gravity, Classical Quantum Gravity **38**, 195002 (2021).

[41] M. Han, Z. Huang, H. Liu, and D. Qu, Complex critical points and curved geometries in four-dimensional Lorentzian spinfoam quantum gravity, Phys. Rev. D **106**, 044005 (2022).

[42] P. Donà, F. Gozzini, and G. Sarno, Searching for classical geometries in spin foam amplitudes: A numerical method, Classical Quantum Gravity **37**, 094002 (2020).

[43] B. Dittrich and S. Steinhaus, Time evolution as refining, coarse graining and entangling, New J. Phys. **16,** 123041 (2014).

[44] S. Steinhaus, Coarse graining spin foam quantum gravity—A review, Front. Phys. **8,** 295 (2020).

[45] S. K. Asante, B. Dittrich, and S. Steinhaus, Spin foams, refinement limit and renormalization, arXiv:2211.09578.

[46] P. Dona, M. Han, and H. Liu, Spinfoams and high performance computing, arXiv:2212.14396.

[47] F. Gozzini, A high-performance code for EPRL spin foam amplitudes, Classical Quantum Gravity **38,** 225010 (2021).

[48] P. Dona and P. Frisoni, How-to compute EPRL spin foam amplitudes, Universe **8,** 208 (2022).

[49] P. Donà and P. Frisoni, Summing bulk quantum numbers with Monte Carlo in spin foam theories, Phys. Rev. D **107,** 106008 (2023).

[50] M. Han, H. Liu, and D. Qu, Complex critical points in Lorentzian spinfoam quantum gravity: 4-simplex amplitude and effective dynamics on double-Δ_3 complex, Phys. Rev. D **108,** 026010 (2023).

[51] C. Allen, F. Girelli, and S. Steinhaus, Numerical evaluation of spin foam amplitudes beyond simplices, Phys. Rev. D **105,** 066003 (2022).

[52] B. Bahr and S. Steinhaus, Investigation of the spinfoam path integral with quantum cuboid intertwiners, Phys. Rev. D **93,** 104029 (2016).

[53] B. Bahr and S. Steinhaus, Numerical Evidence for a Phase Transition in 4d Spin Foam Quantum Gravity, Phys. Rev. Lett. **117,** 141302 (2016).

[54] M. Ali and S. Steinhaus, Toward matter dynamics in spin foam quantum gravity, Phys. Rev. D **106,** 106016 (2022).

[55] J. Engle, E. R. Livine, R. Pereira, and C. Rovelli, LQG vertex with finite Immirzi parameter, Nucl. Phys. **B799,** 136 (2008).

[56] L. Freidel and K. Krasnov, A new spin foam model for 4D gravity, Classical Quantum Gravity **25,** 125018 (2008).

[57] W. Kaminski, M. Kisielowski, and J. Lewandowski, Spin-foams for all loop quantum gravity, Classical Quantum Gravity **27,** 095006 (2010).

[58] B. Bahr and G. Rabuffo, Deformation of the Engle-Livine-Pereira-Rovelli spin foam model by a cosmological constant, Phys. Rev. D **97,** 086010 (2018).

[59] D. Oriti, J. P. Ryan, and J. Thürigen, Group field theories for all loop quantum gravity, New J. Phys. **17,** 023042 (2015).

[60] E. Bianchi, D. Regoli, and C. Rovelli, Face amplitude of spinfoam quantum gravity, Classical Quantum Gravity **27,** 185009 (2010).

[61] A. Riello, Self-energy of the Lorentzian Engle-Pereira-Rovelli-Livine and Freidel-Krasnov model of quantum gravity, Phys. Rev. D **88,** 024011 (2013).

[62] E. R. Livine and S. Speziale, New spinfoam vertex for quantum gravity, Phys. Rev. D **76,** 084028 (2007).

[63] B. Bahr and S. Steinhaus, Investigation of the spinfoam path integral with quantum cuboid intertwiners, Phys. Rev. D **93,** 104029 (2016).

[64] C. Rovelli and F. Vidotto, *Covariant Loop Quantum Gravity: An Elementary Introduction to Quantum Gravity*

and Spinfoam Theory (Cambridge University Press, Cambridge, UK, 2014).

[65] T. E. Regge, General relativity without coordinates, Nuovo Cimento **19,** 558 (1961).

[66] M. Han, Cosmological constant in LQG vertex amplitude, Phys. Rev. D **84,** 064010 (2011).

[67] B. Bahr and G. Rabuffo, Deformation of the Engle-Livine-Pereira-Rovelli spin foam model by a cosmological constant, Phys. Rev. D **97,** 086010 (2018).

[68] G. Calcagni, D. Oriti, and J. Thürigen, Laplacians on discrete and quantum geometries, Classical Quantum Gravity **30** (2013) 125006.

[69] J. Thürigen, Discrete quantum geometries and their effective dimension, Ph.D. thesis, Humboldt-Universität zu Berlin, 2015.

[70] M. Desbrun, A. N. Hirani, M. Leok, and J. E. Marsden, Discrete exterior calculus, arXiv:math/0508341.

[71] H. Sahlmann, Wave propagation on a random lattice, Phys. Rev. D **82,** 064018 (2010).

[72] W. R. Inc., *Mathematica*, Version 13.2.

[73] M. Han, 4-dimensional spin-foam model with quantum Lorentz group, J. Math. Phys. (N.Y.) **52,** 072501 (2011).

[74] V. G. Turaev and O. Y. Viro, State sum invariants of 3 manifolds and quantum 6j symbols, Topology **31,** 865 (1992).

[75] S. Major and L. Smolin, Quantum deformation of quantum gravity, Nucl. Phys. **B473,** 267 (1996).

[76] W. J. Fairbairn and C. Meusburger, Quantum deformation of two four-dimensional spin foam models, J. Math. Phys. (N.Y.) **53,** 022501 (2012).

[77] B. Dittrich, Cosmological constant from condensation of defect excitations, Universe **4,** 81 (2018).

[78] M. Dupuis, L. Freidel, F. Girelli, A. Osumanu, and J. Rennert, On the origin of the quantum group symmetry in 3d quantum gravity, arXiv:2006.10105.

[79] M. Dupuis and F. Girelli, Observables in loop quantum gravity with a cosmological constant, Phys. Rev. D **90,** 104037 (2014).

[80] H. M. Haggard, M. Han, W. Kamiński, and A. Riello, SL (2,C) ChernSimons theory, a non-planar graph operator, and 4D quantum gravity with a cosmological constant: Semiclassical geometry, Nucl. Phys. **B900,** 1 (2015).

[81] M. Han, Four-dimensional spinfoam quantum gravity with a cosmological constant: Finiteness and semiclassical limit, Phys. Rev. D **104,** 104035 (2021).

[82] L. J. Slater, *Generalized Hypergeometric Functions* (Cambridge University Press, Cambridge, England, 1966).

[83] B. Dittrich, Diffeomorphism symmetry in quantum gravity models, Adv. Sci. Lett. **2,** 151 (2009).

[84] B. Bahr and B. Dittrich, (Broken) Gauge symmetries and constraints in Regge calculus, Classical Quantum Gravity **26,** 225011 (2009).

[85] B. Bahr and B. Dittrich, Improved and perfect actions in discrete gravity, Phys. Rev. D **80,** 124030 (2009).

[86] B. Bahr, B. Dittrich, and S. Steinhaus, Perfect discretization of reparametrization invariant path integrals, Phys. Rev. D **83,** 105026 (2011).

[87] A. Perez, Black holes in loop quantum gravity, Rep. Prog. Phys. **80,** 126901 (2017).

[88] D. Benedetti and S. Speziale, Perturbative running of the Immirzi parameter, J. Phys. Conf. Ser. **360,** 012011 (2012).

[89] B. Bahr and V. Belov, On the volume simplicity constraint in the EPRL spin foam model, Phys. Rev. D **97,** 086009 (2018).

[90] M. Assanioussi and B. Bahr, Hopf link volume simplicity constraints in spin foam models, Classical Quantum Gravity **37,** 205003 (2020).

[91] P. Dona and S. Speziale, Asymptotics of lowest unitary SL (2,C) invariants on graphs, Phys. Rev. D **102,** 086016 (2020).

[92] F. Conrady and L. Freidel, On the semiclassical limit of 4d spin foam models, Phys. Rev. D **78,** 104023 (2008).

[93] W. Kaminski, M. Kisielowski, and H. Sahlmann, Asymptotic analysis of the EPRL model with timelike tetrahedra, Classical Quantum Gravity **35,** 135012 (2018).

[94] H. Liu and M. Han, Asymptotic analysis of spin foam amplitude with timelike triangles, Phys. Rev. D **99,** 084040 (2019).

[95] J. D. Simão and S. Steinhaus, Asymptotic analysis of spin-foams with timelike faces in a new parametrization, Phys. Rev. D **104,** 126001 (2021).

[96] M. Han, W. Kaminski, and H. Liu, Finiteness of spinfoam vertex amplitude with timelike polyhedra and the regularization of full amplitude, Phys. Rev. D **105,** 084034 (2022).

[97] V. Bonzom, Spin foam models for quantum gravity from lattice path integrals, Phys. Rev. D **80,** 064028 (2009).

[98] F. Hellmann and W. Kaminski, Holonomy spin foam models: Asymptotic geometry of the partition function, J. High Energy Phys. 10 (2013) 165.

[99] J. R. Oliveira, EPRL/FK asymptotics and the flatness problem, Classical Quantum Gravity **35,** 095003 (2018).

[100] J. S. Engle, W. Kaminski, and J. R. Oliveira, Addendum to 'EPRL/FK asymptotics and the flatness problem', Classical Quantum Gravity **38,** 119401 (2021).

[101] A. Eichhorn and S. Mizera, Spectral dimension in causal set quantum gravity, Classical Quantum Gravity **31,** 125007 (2014).

[102] P. Scott Mara, Triangulations for the cube, J. Comb. Theory Ser. A **20,** 170 (1976).

[103] B. Dittrich and A. Kogios, From spin foams to area metric dynamics to gravitons, Classical Quantum Gravity **40,** 095011 (2023).